

*There is a tide in the affairs of men,
which, taken at the flood, leads on to fortune.
Omitted, all the voyage of their life is bound in shallows and in miseries.
On such a full sea are we now afloat,
and we must take the current when it serves, or lose our ventures.*

William Shakespeare, Julius Caesar, c. 1599.

CHAPTER 20

Structure of the Upper Ocean

In the previous chapter we developed an understanding of the vertically integrated flow of the world's oceans. If we are to proceed further we must develop an understanding of the *vertical structure* of the oceans, and that is the subject of this chapter. Our main focus will be on the upper ocean and we will proceed as follows:

1. We first explore the vertical structure of the wind-driven circulation, largely as a continuation of the investigation of the previous chapter. We use the quasi-geostrophic equations to understand why the subsurface ocean moves at all, and we introduce the notion of potential vorticity homogenization.
2. A limitation of the quasi-geostrophic approach is that these equations take the stratification, $N(z)$, as a given and therefore cannot provide an answer to the question as to what produces the density structure itself. Thus, beginning in Section 20.4, we relax the quasi-geostrophic restriction and, using the *planetary-geostrophic* equations, we try to understand the dynamics that give rise to the vertical structure of density itself. We focus on the *main thermocline*, the region of the upper ocean in which temperature and density vary most rapidly, in all seasons, and we discuss the structure of both the internal thermocline and the ventilated thermocline, the meaning of which will become apparent later.

As with many fluid problems, the dynamics becomes intertwined with the thermodynamics, and the mean flow becomes intertwined with the smaller, turbulent, baroclinic eddies, in rather subtle ways that, to this day, are not fully understood and that large numerical models are only beginning to properly simulate. We begin by looking at the vertical structure of the wind-driven gyres, and if and how the influence of the wind can be communicated to the subsurface ocean.

20.1 VERTICAL STRUCTURE OF THE WIND-DRIVEN CIRCULATION

20.1.1 A Two-layer Quasi-Geostrophic Model

We pose the problem using the quasi-geostrophic equations, taking the background stratification of the ocean as a given.¹ The simplest system that has vertical structure is a two-layer model and that is where we start. We don't yet wish to consider the effects of mesoscale eddies, so we'll limit ourselves to motion larger than the deformation scale, although not so large that the quasi-geostrophic system itself does not hold.

Scales of motion

On scales that are sufficiently larger than the deformation radius we can ignore the relative vorticity compared to planetary vortex stretching and the β -effect. Since quasi-geostrophic scaling itself applies only to scales that are not significantly larger than the deformation scale, our analysis will be formally valid under the following set of inequalities:

$$\begin{aligned}\beta L &\ll f_0 && \text{(small variations in Coriolis parameter),} \\ \beta L &> U/L && \text{(to ignore relative vorticity compared to planetary vorticity),} \\ L^2 &> L_d^2 && \text{(to ignore relative vorticity compared to vortex stretching),} \\ Ro L^2 &\ll L_d^2 && \text{(to keep the variations in stratification small),}\end{aligned}$$

where L_d is the deformation radius and L the scale of the motion. The first and last of the above inequalities are standard quasi-geostrophic requirements, with the ‘ \gg ’ symbol denoting the asymptotic ordering. The middle two inequalities are taken within the quasi-geostrophic dynamics, and are needed in order to ignore relative vorticity and give a balance between the β -effect and vortex stretching. The simultaneous satisfaction of all these conditions may seem restrictive, but the plangent dynamics contained within the quasi-geostrophic equations and the generality of the method employed below will suggest that the principal results obtained may transcend the limitations of the equations used. In the mid-latitude ocean $L_d \approx 10^5$ m and the above inequalities are reasonably well satisfied for $L \approx 10^6$ m and $U \approx 0.1$ m s $^{-1}$ with $\beta = 10^{-11}$ m $^{-1}$ s $^{-1}$ and $f_0 = 10^{-4}$ s $^{-1}$.

Constructing the model

We now make the following simplifications for our model ocean:

- (i) We use the two-layer quasi-geostrophic equations, with layers of equal thickness.
- (ii) We seek only statistically-steady solutions.
- (iii) We include a frictional term coming from a downgradient flux of potential vorticity. Given the neglect of relative vorticity, this is equivalent to an interfacial drag.
- (iv) We neglect the western boundary layer.

Because of the equal-layer-thickness assumption, which makes the algebra simpler, it is best considered as a model for the upper ocean above a level where the vertical velocity is approximately zero. The equations of motion are then

$$J(\psi_1, q_1) = \frac{1}{H_0} \operatorname{curl}_z \boldsymbol{\tau}_T - \nabla \cdot \mathbf{T}_1, \quad J(\psi_2, q_2) = -\nabla \cdot \mathbf{T}_2 \quad (20.1a,b)$$

where

$$q_1 = \beta y + F(\psi_2 - \psi_1), \quad q_2 = \beta y + F(\psi_1 - \psi_2). \quad (20.2a,b)$$

Here, $F = f_0^2/(g' H_0) = 1/L_d^2$ is a measure of the stratification, where H_0 is the thickness of either layer, and the $\nabla \cdot \mathbf{T}$ terms represent interfacial eddy stresses, which, if needed, we will parameterize by a downgradient flux of potential vorticity,

$$\mathbf{T}_1 = -\kappa \nabla q_1 = -\kappa(F \nabla(\psi_2 - \psi_1) + \beta \mathbf{j}), \quad \mathbf{T}_2 = -\kappa \nabla q_2 = -\kappa(F \nabla(\psi_1 - \psi_2) + \beta \mathbf{j}), \quad (20.3)$$

where κ is a constant. We will mostly be interested in the limit of small κ , or more specifically $UL/\kappa \gg 1$, which is a large Péclet number condition. (The Péclet number is similar to a Reynolds number, but with the diffusivity replacing the kinematic viscosity.) So first consider the case when κ is identically zero. An *exact* solution to (20.1) has $\psi_2 = 0$, so that (20.1a) becomes $\beta \partial \psi_1 / \partial x = H_0^{-1} \operatorname{curl}_z \boldsymbol{\tau}_T$, with solution

$$\psi_1 = -\frac{1}{H_0 \beta} \int_x^{x_E} \operatorname{curl}_z \boldsymbol{\tau}_T dx. \quad (20.4)$$

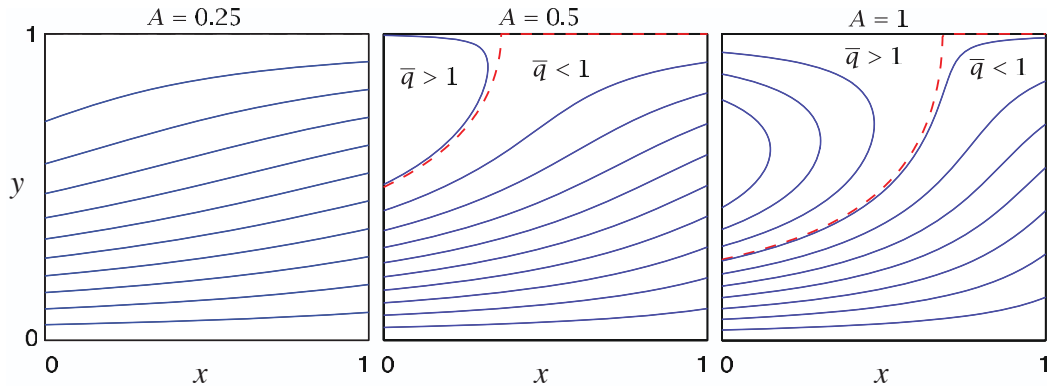


Fig. 20.1 Contours of $\bar{q} = \beta y + A \sin \pi y(1 - x)$, with $\beta = 1$, for three values of A . The red dashed line is $\bar{q} = 1$, which separates the blocked region to the east ($\bar{q} < 1$) from the closed region to the west ($\bar{q} > 1$). See Fig. 20.2 for plots of the other fields.

That is, *there is no flow in the lower layer*, and the upper layer solution is given by Sverdrup balance. The solution satisfies $\psi_1 = 0$ at $x = x_E$ and, because $\psi_2 = 0$, the nonlinear term on the left-hand side of (20.1a) vanishes identically. This is both counter-intuitive and counter-observations, for we know the subsurface ocean is not quiescent. Is there another solution?

A general solution

We now construct the solution without assuming $\psi_2 = 0$. Although the equations are nonlinear, we can obtain a linear equation for a streamfunction by adding (20.1a) and (20.1b), giving

$$J(\psi_1, \beta y + F(\psi_2 - \psi_1)) + J(\psi_2, \beta y + F(\psi_1 - \psi_2)) = \frac{1}{H_0} \operatorname{curl}_z \boldsymbol{\tau}_T. \quad (20.5)$$

The nonlinear terms cancel leaving

$$J(\bar{\psi}, \beta y) = \frac{1}{H_0} \operatorname{curl}_z \boldsymbol{\tau}_T, \quad \text{where } \bar{\psi} = \psi_1 + \psi_2, \quad (20.6a,b)$$

with solution, as in (20.4),

$$\bar{\psi} = -\frac{1}{H_0 \beta} \int_x^{x_E} \operatorname{curl}_z \boldsymbol{\tau}_T dx'. \quad (20.7)$$

This simply says that the vertically integrated flow obeys Sverdrup balance. For the canonical wind stress

$$\boldsymbol{\tau}_T = -\tau_0 \cos \pi y \mathbf{i}, \quad (20.8)$$

and we obtain $\bar{\psi} = (\pi \tau_0 / \beta H_0)(x_E - x) \sin \pi y$. It is useful to define

$$\bar{q} \equiv (\beta y + F\bar{\psi}), \quad (20.9)$$

and then $\bar{q} = \beta[y + A(1 - x) \sin \pi y]$, where $A = \pi \tau_0 / (\beta H_0)$ parameterizes the wind strength, and this is plotted in Fig. 20.1. For $\bar{q} < 1$ (below and to the right of the dashed line) all the geostrophic contours intersect the eastern boundary and the flow is ‘blocked’. For $\bar{q} > 1$ the flow is ‘closed’.

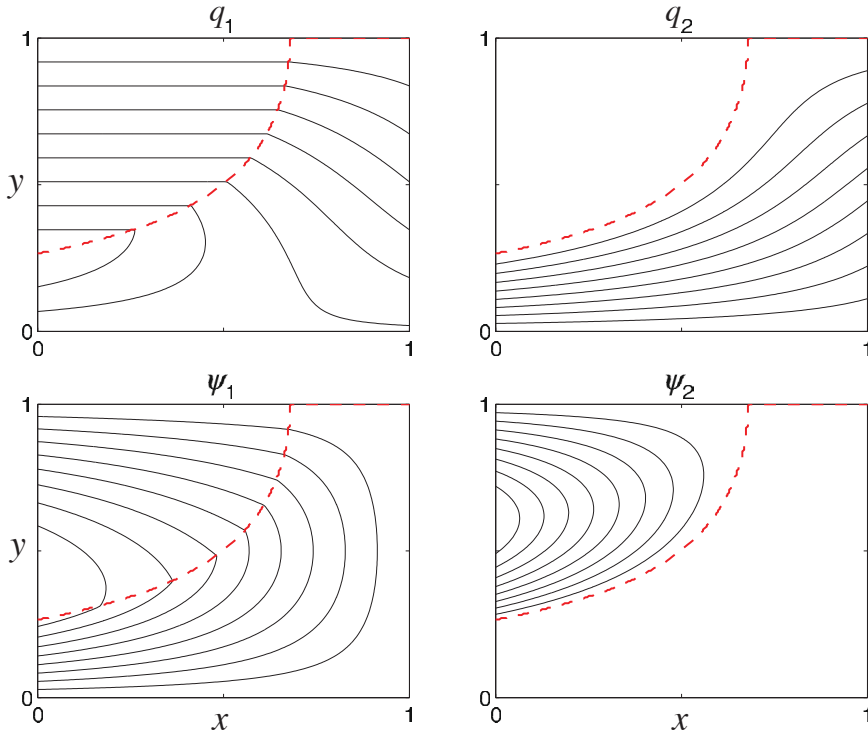


Fig. 20.2 Upper- and lower-level potential vorticity and streamfunction for the canonical wind stress (20.8). The field of \bar{q} is that of Fig. 20.1 with $A = 1$. The dashed line divides the blocked region from the closed region. The lower layer streamfunction ψ_2 is non-zero only in the closed region, and here $q_2 = \beta L$ and $q_1 = 2\beta y - \beta L$. In the blocked region the upper layer carries all of the Sverdrup transport. Both the streamfunction and potential vorticity are continuous at the divide: $\psi_2 = 0$ and $q_2 = \bar{q} = \beta L$.

Lower layer

Although the full equations are nonlinear, using (20.9) we can obtain a linear equation for the lower layer. Because the Jacobian of a field with itself vanishes, (20.1b) and (20.2b) imply that

$$J(\psi_2, \bar{q}) = -\nabla \cdot \mathbf{T}_2, \quad (20.10)$$

and this is useful because \bar{q} is a function of the wind, using (20.9). If $\nabla \cdot \mathbf{T}_2 = 0$ then

$$J(\psi_2, \bar{q}) = 0. \quad (20.11)$$

As well as the possibility that $\psi_2 = 0$ we now have the more general solution

$$\psi_2 = G(\bar{q}), \quad (20.12)$$

where G is an *arbitrary* function of its argument. Isolines of ψ_2 and \bar{q} are then coincident. (Contours that are isolines of both streamfunction and potential vorticity are known as geostrophic contours.)

Consider a blocked isoline of \bar{q} ; that is, one that intersects the eastern boundary (see Fig. 20.1). The ψ_2 contour coincident with this has a value of zero at the eastern boundary (by the no-normal flow condition). Thus $\psi_2 = 0$ *everywhere* in the blocked region, and $q_2 = \bar{q}$. In this region the Sverdrup transport is carried everywhere by the upper layer, and the lower layer is at rest. This

Summary of Wind-Driven, Two-layer Solution

The vertically integrated flow in a wind-driven two-layer quasi-geostrophic model is determined by Sverdrup balance. The effects of eddies may be crudely parameterized by a downgradient diffusion of potential vorticity. If this is identically zero, then the lower-layer flow is identically zero and the upper-layer flow carries all the transport. If the diffusion is small but non-zero, the lower-layer streamfunction approximately satisfies $J(\psi_2, \bar{q})$, where \bar{q} is given by (20.9), and therefore ψ_2 is a function of \bar{q} — that is, $\psi_2 \approx G(\bar{q})$. For a typical subtropical wind, contours of \bar{q} , and therefore contours of ψ_2 , are naturally divided into two regions (Fig. 20.1):

- (i) A blocked region (the shadow zone), in which contours of \bar{q} intersect the eastern boundary, the lower layer flow is zero and the upper layer carries all the Sverdrup transport.
- (ii) A closed region in which (if we envision a nearly inviscid western boundary current) the flow recirculates. In this region we posit that the lower layer potential vorticity becomes homogeneous, with a value determined by the value at the region's boundary, and this in turn is determined by tracing \bar{q} back to the domain boundary.

To satisfy a circulation constraint the function $G(\bar{q})$ must be a linear function, and given this, the entire solution may be determined. If, for example, the wind is zonal and a function of y only, and $\text{curl}_z \tau_T = g(y)$ then, in both regions:

$$\bar{\psi} \equiv \psi_1 + \psi_2 = -\frac{1}{\beta H_0} g(y)(x_E - x), \quad \bar{q} \equiv \beta y + F\bar{\psi}. \quad (\text{OC.1a,b})$$

In the blocked region:

$$\psi_2 = 0, \quad \psi_1 = -\frac{1}{\beta H_0}(x_E - x)g(y), \quad (\text{OC.2a})$$

$$q_1 = \beta y + F(\psi_1 - \psi_2), \quad q_2 = \beta y + F(\psi_2 - \psi_1). \quad (\text{OC.2b})$$

In the closed region:

$$q_2 = \beta L \quad (\text{by homogenization}), \quad (\text{OC.3a})$$

$$\psi_2 = \frac{1}{2F}(\bar{q} - \beta L), \quad \psi_1 = \bar{\psi} - \psi_2, \quad (\text{OC.3b})$$

$$q_1 = \beta y + F(\psi_2 - \psi_1) = 2\beta y - \beta L. \quad (\text{OC.3c})$$

For $g(y) = -\sin \pi y$ these solutions are illustrated in Figs. 20.1 and 20.2.

This approach provides a solution to the conundrum of what drives the subsurface (quasi-geostrophic) ocean, for if there are no eddy effects at all (i.e., in (20.3) $T_1 = T_2 = 0$), then the lower layer flow is stationary. This solution is not wholly realistic, for the upper layer flow could be made quite shallow. Another solution to this issue is provided in Section 20.7, wherein it is assumed that the lower layers may outcrop and so feel the wind directly.

region is called a ‘shadow zone’, for the fluid is in the shadow of the eastern boundary, and it will re-appear in a model of the ventilated thermocline later on in this chapter. In the region of closed contours, ψ_2 cannot be given by this argument. But if κ is sufficiently small, we can expect (20.11) to approximately hold, and that the presence of a small amount of dissipation will determine the functional relationship between ψ_2 and \bar{q} . Thus, in summary, there are two regions of flow:

- (i) the blocked region in which $\psi_1 \approx \bar{\psi} \gg \psi_2$ and ψ_1 is approximately given by (20.4);
- (ii) a closed region in which $\psi_2 = G(\bar{q}) + \mathcal{O}(\kappa)$.

20.1.2 Relation Between Streamfunction and Potential Vorticity

A general argument

In Chapter 13 we showed that, within a region of closed contours, the values of a tracer that is materially conserved except for the effects of a small diffusion would become *homogeneous*. In the case at hand, potential vorticity is that tracer, so that within potential vorticity contours or closed streamlines potential vorticity will become homogenized. If we can determine the value of q_2 within the region of closed contours, then from (20.2) ψ_2 is given by

$$\psi_2 = (1/2F)(\bar{q} - q_2), \quad (20.13)$$

and the solution would be complete. Now, outside the closed region $\psi_2 \ll \psi_1$, so that the outermost contour of the closed region must be characterized by $q_2 \approx \bar{q}$, for this makes ψ_2 continuous between closed and blocked regions. Thus, the value of q_2 within the closed homogeneous region is that of \bar{q} (i.e., $\beta y + F\bar{\psi}$) on its boundary. Since this contour intersects the poleward edge of the domain, where $\bar{\psi}$ is zero, the value of this contour is just βy at $y = L$; that is, βL . Thus, within the closed region,

$$q_2 = \beta L. \quad (20.14)$$

A specific calculation

Now consider the steady, lower-layer potential vorticity equation (20.1b); noting that $J(\psi_2, F(\psi_1 - \psi_2)) = J(\psi_2, F(\psi_1 + \psi_2))$, (20.1b) may be written as

$$J(\psi_2, \bar{q}) = -\nabla \cdot \mathbf{T}_2. \quad (20.15)$$

Integrating around a closed contour of \bar{q} the left-hand side vanishes and

$$R \int (\nabla \psi_1 - \nabla \psi_2) \cdot \mathbf{n} \, dl = 0 \quad \text{or} \quad \oint \mathbf{u}_1 \cdot dl = \oint \mathbf{u}_2 \cdot dl. \quad (20.16a,b)$$

Thus, the deep circulation around a mean geostrophic contour (i.e., isoline of \bar{q}) is equal to the upper-level circulation.

Previously we argued that

$$\psi_2 = G(\bar{q}) = G(\beta y + F(\psi_1 + \psi_2)), \quad (20.17)$$

where G is an arbitrary function of its argument. In order to satisfy (20.16) (a linear relation between \mathbf{u}_1 and \mathbf{u}_2) G must be a linear function, and so we write

$$\psi_2 = C \left[\frac{\beta y}{F} + (\psi_1 + \psi_2) \right] + B, \quad (20.18)$$

where C and B are constants. This may be rearranged to give

$$\psi_1 = -C \frac{\beta y}{F} + (\psi_1 + \psi_2)(1 - C) - B. \quad (20.19)$$

The above two equations are consistent with (20.16) if $C = 1/2$. With this, (20.18) gives

$$\bar{q} = 2F(\psi_2 - B), \quad (20.20)$$

and the potential vorticity in the closed contour region of the lower layer is

$$q_2 = \beta y + F\bar{\psi} - 2F\psi_2 = -2FB. \quad (20.21)$$

That is, it is constant. Outside the closed contours $\psi_2 \ll \psi_1$ so that $q_2 \approx \bar{q} = \beta y + F\psi_1$. If we trace this contour to the edge of the domain where $\psi_1 = 0$ and $y = L$ then we see that the value of \bar{q} on the contour, and hence q_2 in the closed region, is βL , as in (20.14), and $B = -\beta L/(2F)$. Using (20.20) then gives

$$\psi_2 = (2F)^{-1}(\bar{q} - \beta L). \quad (20.22)$$

Given ψ_2 and q_2 , from (20.14), we obtain q_1 and ψ_1 using (20.2) and (20.6b), giving

$$q_1 = 2\beta y - \beta L, \quad \psi_1 = \bar{\psi} - \psi_2. \quad (20.23)$$

All these fields are illustrated in Fig. 20.2, and see the shaded box on page 765 for a summary.

20.2 ♦ A MODEL WITH CONTINUOUS STRATIFICATION

We now look at the dynamics of the continuously stratified circulation, largely by way of an extension of our two-layer procedure. Let us first consider how deep the wind's influence is.

20.2.1 Depth of the Wind's Influence

The thermal wind relationship in the form $f \partial u / \partial z = \partial b / \partial y$ implies a vertical scale H given by

$$H = \frac{fUL}{\Delta b}, \quad (20.24)$$

where Δb is a typical magnitude of the horizontal variation of the buoyancy. We can relate this to the Ekman pumping velocity W_E using the linear geostrophic vorticity equation, $\beta v = f \partial w / \partial z$, which, (assuming that the horizontal components of velocity are roughly similar, i.e., $V = U$), implies that

$$U = \frac{fW_E}{\beta H}. \quad (20.25)$$

Equations (20.24) and (20.25) may be combined to give an estimate of the depth of the wind-driven circulation, namely

$$H = \left(\frac{f^2 W_E L}{\beta \Delta b} \right)^{1/2}, \quad (20.26)$$

where L may be interpreted as the gyre scale. We now use quasi-geostrophic scaling to relate the horizontal temperature gradient to the stratification using the thermodynamic equation,

$$\frac{Db}{Dt} + wN^2 = 0, \quad (20.27)$$

with implied scaling

$$\Delta b = \frac{W_E N^2 L}{U} = \frac{N^2 \beta H L}{f_0}, \quad (20.28)$$

where the second equality uses (20.25). Using (20.26) and (20.28) gives

$$H = \left(\frac{W_E f^3}{\beta^2 N^2} \right)^{1/3}. \quad (20.29)$$

Potential vorticity interpretation

The estimate (20.29) can be obtained and interpreted more directly: *the wind-driven circulation penetrates as far as it can alter the potential vorticity q from its planetary value βy .* Recall that, ignoring relative vorticity,

$$q = \beta y + \frac{\partial}{\partial z} \left(\frac{f_0^2}{N^2} \frac{\partial \psi}{\partial z} \right). \quad (20.30)$$

The two terms are comparable if

$$\frac{f_0^2}{N^2 H^2} U L \approx \beta L \quad \text{or} \quad H^2 \approx \frac{f_0^2 U}{N^2 \beta}. \quad (20.31)$$

Using (20.25) to eliminate U in favour of W_E recovers (20.29). Thus, for a given stratification, we have an estimate of the depth of the wind-driven circulation, or at least a scaling for depth of the vertical influence of the wind.

20.2.2 The Complete Solution

Armed with an estimate for the depth of the wind's influence, we can obtain a solution for the continuously stratified case analogous to that found in the two-layer case in Section 20.1. Our assumptions are as follows:

- (i) In the limit of small dissipation, streamfunction and potential vorticity have a functional relationship with each other.
- (ii) Potential vorticity is homogenized within closed isolines of q or ψ . The value of q within the homogenized pool is that of the outermost contour, which here is the value of q at the poleward edge of the barotropic gyre.
- (iii) Outside of the pool region, (i.e., below the depth of the wind's influence) the streamfunction is zero, and the potential vorticity is given by the planetary value, i.e., βy .

Given these, finding a solution is not difficult. If N^2 is constant and neglecting relative vorticity, the expression for potential vorticity is

$$q = \frac{\partial^2}{\partial z^2} \left(\frac{f_0^2}{N^2} \psi \right) + \beta y. \quad (20.32)$$

We nondimensionalize by writing

$$z = \left(\frac{f_0^2 U}{N^2 \beta} \right)^{1/2} \hat{z}, \quad q = \beta L \hat{q}, \quad \psi = \hat{\psi} U L, \quad y = L \hat{y}, \quad w = \frac{U^2 f_0}{N^2 H} \hat{w}, \quad (20.33)$$

where the hatted variables are nondimensional, and the scaling for w arises from the thermodynamic equation $N^2 w \sim J(\psi, f_0 \psi_z)$. With this, (20.32) becomes

$$\hat{q} = \frac{\partial^2 \hat{\psi}}{\partial \hat{z}^2} + \hat{y}. \quad (20.34)$$

The flow is then given by solving the following equations:

$$\psi_{zz} + y = y_0, \quad -D(x, y) < z < 0, \quad (20.35a)$$

$$\psi = 0, \quad z \leq -D(x, y), \quad (20.35b)$$

where D is the (to be determined) depth of the bowl, y_0 is a constant, and we have dropped the hats over the nondimensional variables. The solution in $D(x, y) < z < 0$ corresponds to the closed

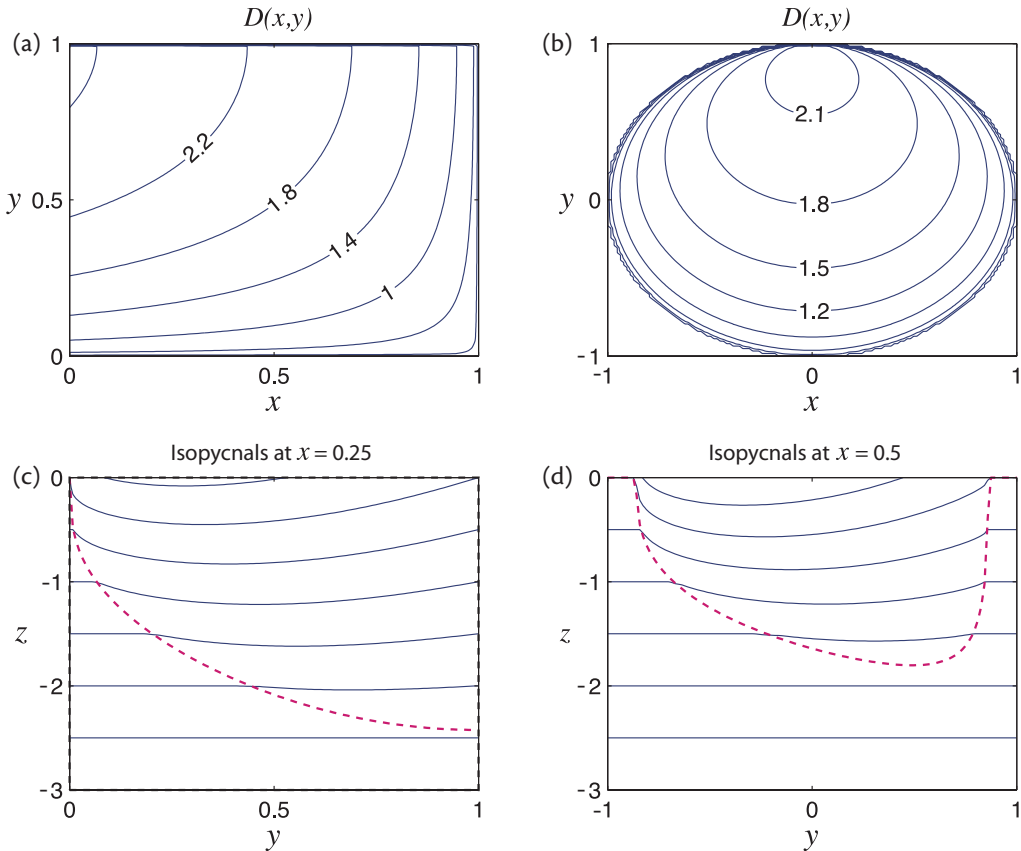


Fig. 20.3 Solutions of (20.9) for two different barotropic streamfunctions. On the left $\psi_B = (1 - x) \sin \pi y$ and on the right $\psi_B = 1 - (x^2 + y^2)$ for $x^2 + y^2 < 1$, zero elsewhere. The upper panels show contours of the depth of the wind-influenced region [solutions of (20.40)]. The depth increases to the northwest in the left panel, and to the north in the right panel, so that in both cases the area of the bowl shrinks with depth. The lower panels are contours of $z + (\beta L / f_0) \psi_z / 2$, with $\beta L / f_0 = 1/2$, obtained from (20.36) or (20.41), at $x = 0.25$ and $x = 0.5$ in the two cases. These are isopycnal surfaces, with a rather large value of $\beta L / f_0$ to exaggerate the displacement in the bowl region. The dashed lines indicate the boundary of the bowl region, outside of which the isopycnals are flat.

region of the two-layer model, and the solution $z \leq -D(x, y)$ corresponds to the blocked region of zero lower-layer flow. The constant y_0 is the nondimensional value of potential vorticity within the pool region, and following our reasoning in the two-layer case this is the value of the potential vorticity at the northern boundary. Dimensionally this is βL , so that in nondimensional units $y_0 = 1$.

The lower boundary condition on (20.35a) is that $\psi = \psi_z = 0$ at $z = -D$, because in the abyss $\psi = \partial\psi/\partial z = 0$ and we require that both ψ and $\partial\psi/\partial z$ be continuous (note that the buoyancy perturbation is proportional to $\partial\psi/\partial z$). The solution that satisfies this is

$$\psi = \frac{1}{2}(z + D)^2(y_0 - y), \quad (20.36)$$

and $\psi = 0$ for $z < -D$.

To obtain an expression for D we first note that the nondimensional vertical velocity at $z = 0$

is given by

$$w = -J(\psi, \psi_z), \quad (20.37)$$

which, using (20.36), gives

$$w = \frac{1}{2}(z + D)^2(y_0 - y) \frac{\partial D}{\partial x}. \quad (20.38)$$

At $z = 0$ the vertical velocity is the Ekman pumping velocity and (20.38) becomes

$$D^2 \frac{\partial D}{\partial x} = \frac{2w_E}{(y_0 - y)}. \quad (20.39)$$

But the Ekman pumping velocity is related to the barotropic streamfunction, ψ_B , by the Sverdrup relationship, so that integrating (20.39) gives

$$D^3 = \frac{6\psi_B}{(y_0 - y)} = -\frac{6(x_E - x)w_E}{(y_0 - y)}, \quad (20.40)$$

where the second equality holds if w_E is not a function of x . This is a solution for the depth of moving region, the bowl in which potential vorticity is homogenized. An expression for the streamfunction is then obtained by using (20.40) in (20.36), and is found to be

$$\psi = \begin{cases} \frac{1}{2} [z(y_0 - y)^{1/2} + (6\psi_B)^{1/3}(y_0 - y)^{1/6}]^2 & -D < z < 0, \\ 0 & z < -D. \end{cases} \quad (20.41)$$

The potential vorticity corresponding to this solution is

$$q = \begin{cases} y_0 & -D < z < 0, \\ y & z < -D. \end{cases} \quad (20.42)$$

Solutions are illustrated in Figs. 20.3 for cases with two different barotropic streamfunctions.

It is possible to heuristically extend models such as the one described above by appending a western boundary layer, and indeed the homogenization of potential vorticity depends upon the presence of such a region to allowing the flow to recirculate. However, as we saw in Section 19.5.3, it is difficult for flow to leave a western boundary layer without the help of friction, and a neutrally stable, damped, stationary Rossby wave typically forms. The critical issue then is whether the presence of dissipation in the western boundary layer affects the homogenization of potential vorticity in the gyre itself. This problem is the province of observation and numerical simulation, and solutions with both quasi-geostrophic and primitive equation models do in fact show that potential vorticity is able to homogenize under many circumstances.³ Let us now take a brief look at some observations.

20.3 OBSERVATIONS OF POTENTIAL VORTICITY

Homogenization of potential vorticity in the real ocean has been observed in both Pacific and Atlantic Oceans, in both hemispheres, and to a lesser degree in the Indian Ocean, and various maps are shown in Fig. 20.4 through Fig. 20.7.⁵ In all of the plots we see that the near-equatorial variation of potential vorticity is dominated by the beta effect, more so at depth where the potential vorticity isolines are more-or-less along latitude lines until almost 20°, but in the subtropical gyres there are large regions of homogeneous potential vorticity.

Looking first at the Pacific, the upper two plots in Fig. 20.4 show the potential vorticity (here defined as $f\partial\rho/\partial z$) on potential density surfaces in the main thermocline. These surfaces slope

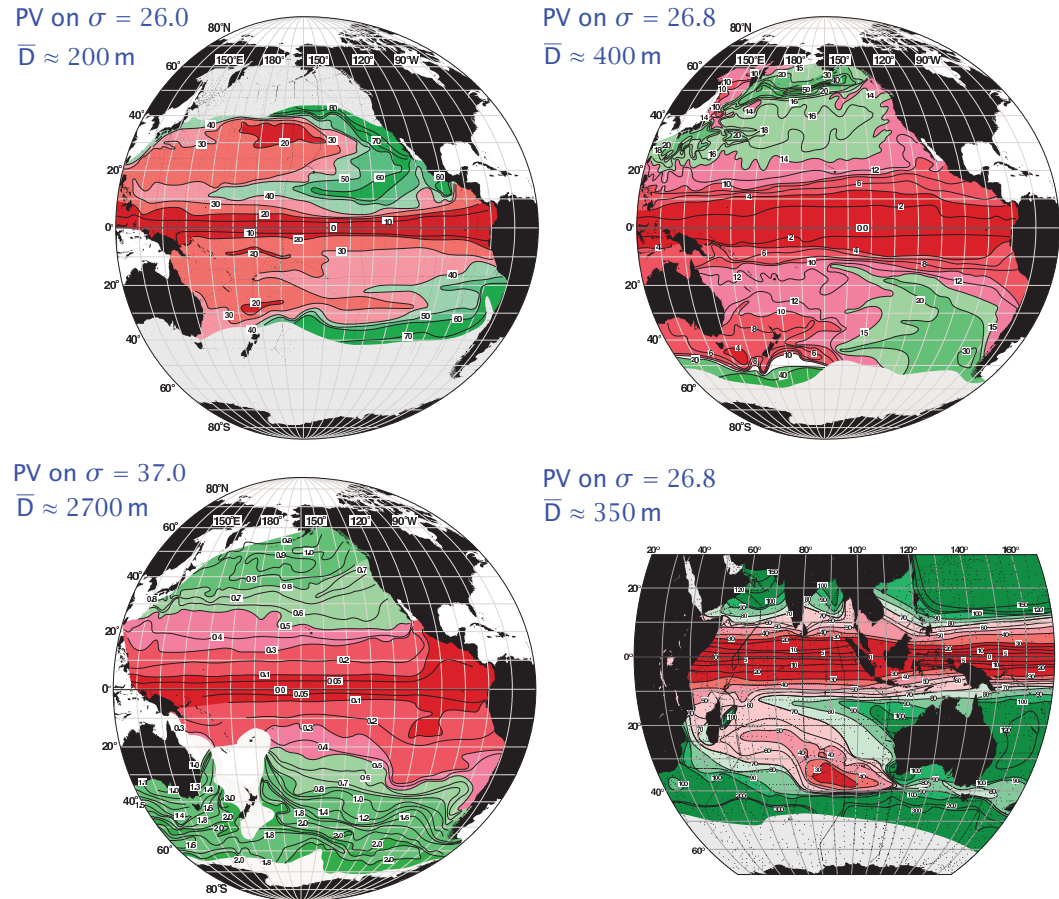


Fig. 20.4 Potential vorticity (i.e., $f(\partial\rho/\partial z)$) in the Pacific and Indian Oceans on the potential density surfaces labelled, which each have approximate average depths D . Some potential vorticity homogenization can be seen in the subtropical gyre in the Pacific (the upper two plots) but less so at depth in the Pacific (lower left) and less so at all depths in the Indian Ocean (just the upper ocean is shown, lower right), which has a less pronounced gyre structure.²

up toward the pole, and the $\sigma = 26$ surface (i.e., a surface with a potential density of approximately 1026 kg m^{-3}) outcrops at about 40° , a little equatorward of the boundary between the subpolar and subtropical gyre. On these surfaces there are large swathes of near-uniform potential vorticity in the subtropical gyre, perhaps a little more obviously so in the Northern Hemisphere, with strong gradients quite noticeable at the gyre edge at about 50° N. Tongues of high potential vorticity are advected by the gyre itself, sweeping equatorward and westward along the $\sigma = 26$ surface in the Northern Hemisphere.

Moving into the deep Pacific there is less homogenization, with isolines of potential vorticity generally crossing the entire Pacific at all latitudes, with just the odd pool of closed contours. The Indian Ocean has less potential vorticity homogenization at all depths, most likely because the subtropical gyre itself is less pronounced in the Indian Ocean, and the subpolar gyre is largely replaced by the eastward flow of the Antarctic Circumpolar Current system.

The Atlantic also shows large regions of homogenization in the upper ocean as seen in Fig. 20.5 and Fig. 20.6. These maps were constructed from a different set of observations, and using a different method, than those of Fig. 20.4, but show similar features — homogenization in the upper gyre

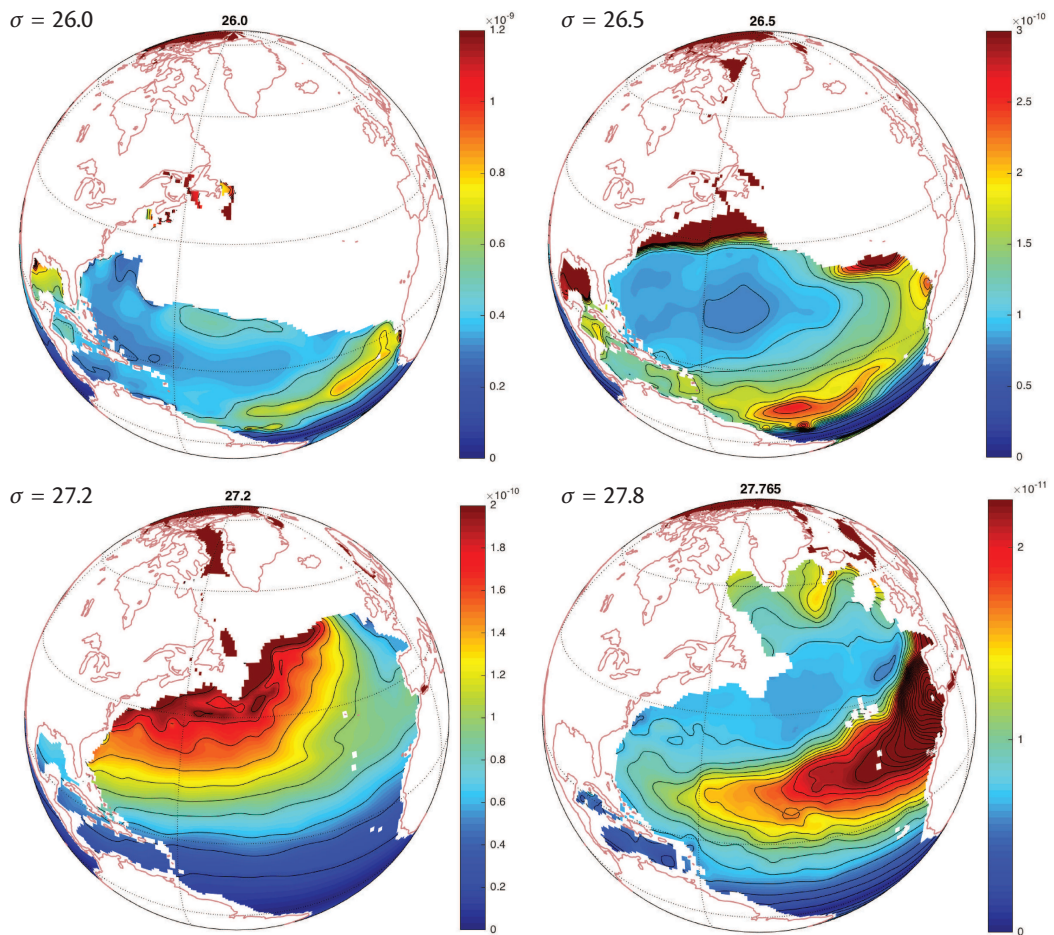


Fig. 20.5 Potential vorticity in the Atlantic Ocean on the potential density surfaces labelled, averaged over several Januaries using the MIMOC climatology. Potential vorticity is a normalized version of f/h . Specifically it is $|f|\delta\sigma/(\rho h)$ where $h(x, y)$ is the isopycnal layer thickness and $\delta\sigma$ is a fixed difference between layer interface potential densities, so here PV has units of $\text{m}^{-1}\text{s}^{-1}$. The PV is homogenized over much of the subtropical gyre around $\sigma = 26.5$. At deeper levels the potential vorticity is more dominated by the beta effect and an influx of Mediterranean water.⁴

but planetary values (and now a Mediterranean influence) dominating at depth. Consider Fig. 20.5 layer-by-layer, from the top down, where a close inspection of Fig. 20.8 will reveal the depths of each layer. The shallow, $\sigma = 26.0$ layer (typically tens of metres deep) outcrops in the middle of the subtropical gyre, receiving most of its fluid directly by Ekman-pumping from the mixed layer, and has a relatively small pool of homogenized potential vorticity. The deeper, $\sigma = 26.5$ level (with typical depths of a few hundred metres over much of the gyre) outcrops much further poleward and consequently has an extensive recirculating regime that homogenizes the potential vorticity. We also see a region between about 10°N and 25°N where potential vorticity increases moving southward — that is, $\partial Q/\partial y < 0$ — so enabling baroclinic instability. Going deeper, at $\sigma = 27.24$ (with typical depth of several hundred to a thousand or so metres) the planetary influence begins to dominate, with the subtropical gyre shrinking and a smaller region of potential vorticity homogenization further north. Finally, at $\sigma = 27.76$, or about 1500 m depth, the circulation is dominated by low potential vorticity Labrador Sea Water to the north and high potential vorticity

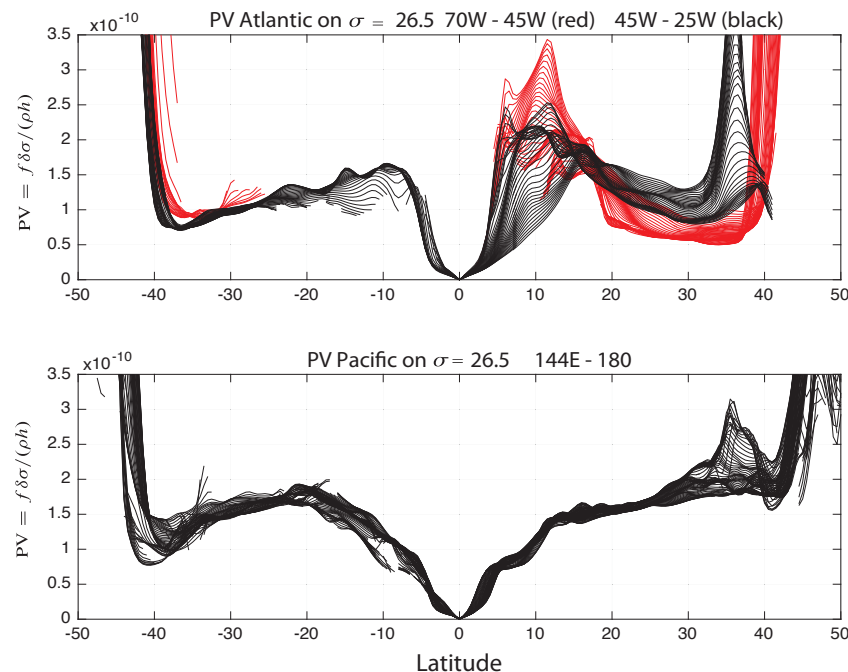


Fig. 20.6 Potential vorticity in the Atlantic and Pacific at the $\sigma_0 = 26.5$ level, using the same data as in Fig. 20.5.⁴ The Coriolis parameter is latitudinally varying but taken as positive in both hemispheres for graphical convenience. See text for more discussion.

from Mediterranean Salt Tongue to the south — again with a potentially baroclinically unstable flow where potential vorticity increases equatorward. The homogenization in both Pacific and Atlantic is very strikingly displayed in Fig. 20.6 and Fig. 20.7, with broad plateaus of near-constant potential vorticity reaching to the poleward edge of the gyres, where there is a sudden leap that acts as a mixing barrier.

The story of potential vorticity is a rich one. The mesoscale eddies provide the stirring that leads to the homogenization, but competing processes complicate the picture. The eddies weaken with depth and planetary effects begin to dominate, and in the upper ocean the varied influences of the western boundary current, topographic effects and the stripping of potential vorticity sheets from solid boundaries turn the ocean into a complex tapestry.

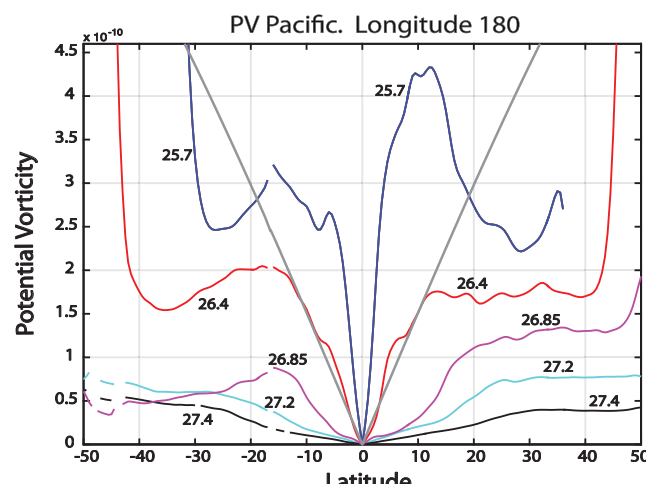


Fig. 20.7 As for Fig. 20.6, but now showing the potential vorticity at various sigma levels in the Pacific, on the date line at longitude 180. The v-shaped grey lines show the reference variation due to βy for the $\sigma = 26.4$ level. For the other levels, the reference variation is similar to the actual variation between about 0° and 10° latitude.

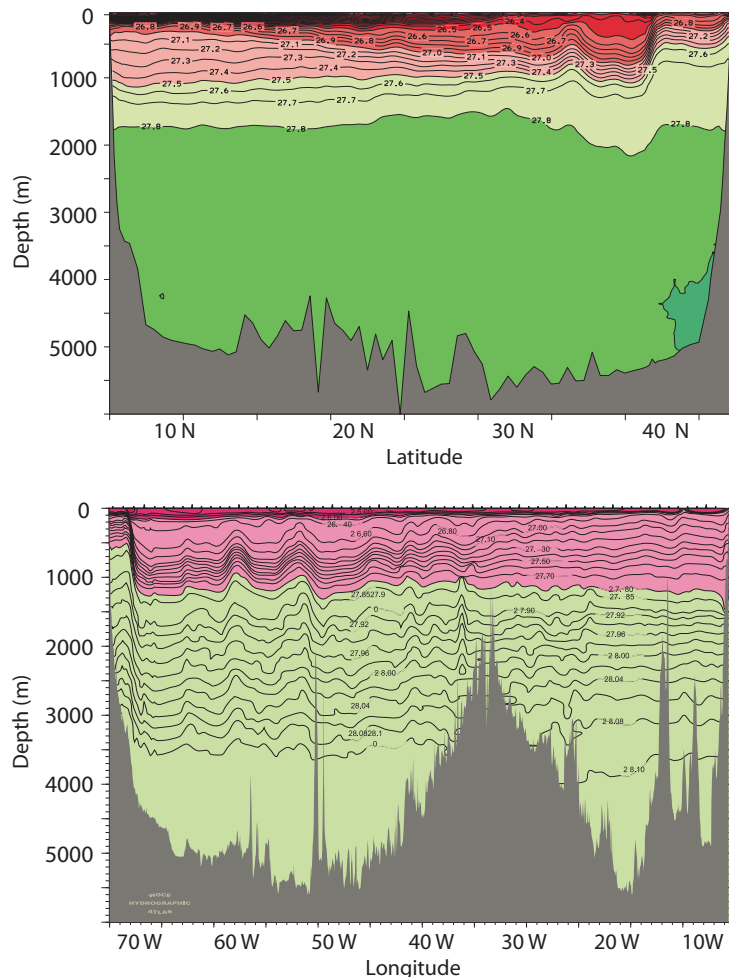


Fig. 20.8 Sections of density in the North Atlantic.

Upper panel: meridional section of potential density at 53°W, from 5°N to 45°N, with a uniform contour interval. In the upper northwestern region of the subtropical thermocline there is a region of low stratification known as MODE water: isopycnals above this outcrop in the subtropical gyre and are ‘ventilated’; isopycnals below the MODE water outcrop in the subpolar gyre, north of about 45°, and/or in ACC.

Lower panel: zonal section of neutral density at 36°N, from about 75°W to 10°W. Contour interval changes where the colour changes. Note the front associated with the western boundary current at about 70°W.⁶

20.4 THE MAIN THERMOCLINE

We now approach the dynamics of the upper ocean from another angle and address the mechanisms that give rise to the actual density structure of the upper ocean, and in particular to the *main thermocline*, which is the region of the upper ocean, about 1 km deep, in which the density and temperature change most rapidly, as illustrated in Fig. 20.8 and Fig. 20.9.

We will consider the circulation in a closed, single hemispheric basin, and suppose that there is a net surface heating at low latitudes and a net cooling at high latitudes that maintains a meridional temperature gradient at the surface. Let us presume, *ab initio*, that there is a single overturning cell, with water rising at low latitudes before returning to polar regions, as illustrated schematically in Fig. 20.10. We will investigate the dynamics of this meridional overturning circulation (MOC) in much more detail in the next chapter, but here our interest is mainly in why and how affects the density structure in the upper ocean and this is less affected by interhemispheric effects. (Readers for whom the MOC is of primary interest may wish to read Chapter 21 before proceeding.) We will also, by and large, omit considerations of saline effects and assume a linear equation of state, so that the thermocline is synonymous with the *pycnocline*, the region where density changes rapidly.

The physical picture we have is the following. Cold, dense water at high latitudes sinks, so that dense water extends all the way to the ocean floor. By hydrostasy the pressure in the deep ocean is then higher at high latitudes than at low, where the water is warmer. Thus the water moves

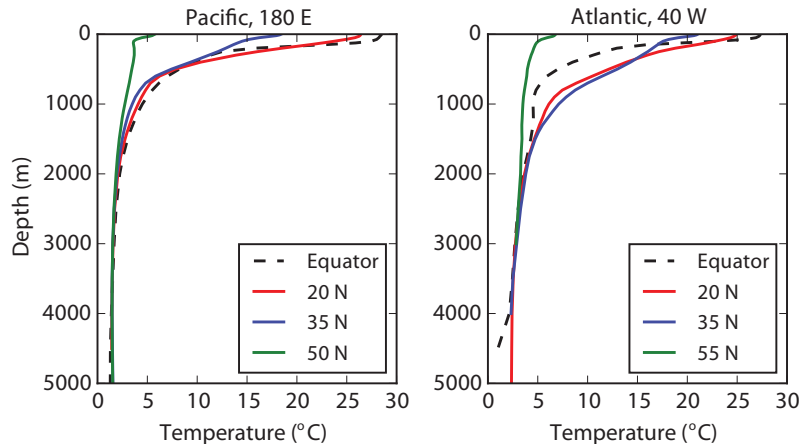


Fig. 20.9 Profiles of mean temperature in the North Pacific and Atlantic, from woe, at the longitudes and latitudes indicated. The profiles are considerably smoother than instantaneous ones.

Note the shallowness of the equatorial thermoclines (especially in the Atlantic), and weakness of the subpolar thermoclines.

equatorward filling the abyss. This water is also slowly *warmed* by heat diffusion down from above, and it is this diffusion that enables the circulation to persist: if diffusion were zero, the entire ocean would eventually fill with the densest available water and the circulation would cease. The water that fills the interior from the cold pole is colder and denser than the surface waters at lower latitude so there must be a vertical temperature gradient, except at the highest latitudes where the water is sinking, and we indeed see in Fig. 20.9 how the vertical temperature profile varies with latitude. However, without considering the dynamics it is hard to see what form the temperature profile will take; for example, it is conceivable that the polar waters might fill up the abyss nearly all the way to the surface, leaving a thermocline only a few metres thick. Or there might be a uniform temperature gradient from the surface to the ocean floor.

Complicating matters, the thermocline is also the region where the gyre circulation is most prominent, so that the potential vorticity dynamics of the previous few sections must play a role. Putting that complication aside for now, let us first look at a simple kinematic model.

20.4.1 A Simple Kinematic Model

The fact that cold water with polar origins upwells into a region of warmer water suggests that we consider the simple one-dimensional advective-diffusive balance,

$$w \frac{\partial T}{\partial z} = \kappa \frac{\partial^2 T}{\partial z^2}, \quad (20.43)$$

where w is the vertical velocity, κ is a diffusivity and T is temperature. In mid-latitudes, where this might hold, w is positive and the equation represents a balance between the upwelling of cold water and the downward diffusion of heat. If w and κ are given constants, and if T is specified at the top ($T = T_T$ at $z = 0$) and if $\partial T / \partial z = 0$ at great depth ($z = -\infty$) then the temperature falls exponentially away from the surface according to

$$T = (T_T - T_B) e^{wz/\kappa} + T_B, \quad (20.44)$$

where T_B is the temperature at depth. Temperature decays exponentially away from its surface value with the scale

$$\delta = \frac{\kappa}{w}, \quad (20.45)$$

and this is an estimate of the thermocline thickness. It is not particularly useful, because the magnitude of w depends on κ , as we will see. However, it is reasonable to see if the observed ocean is

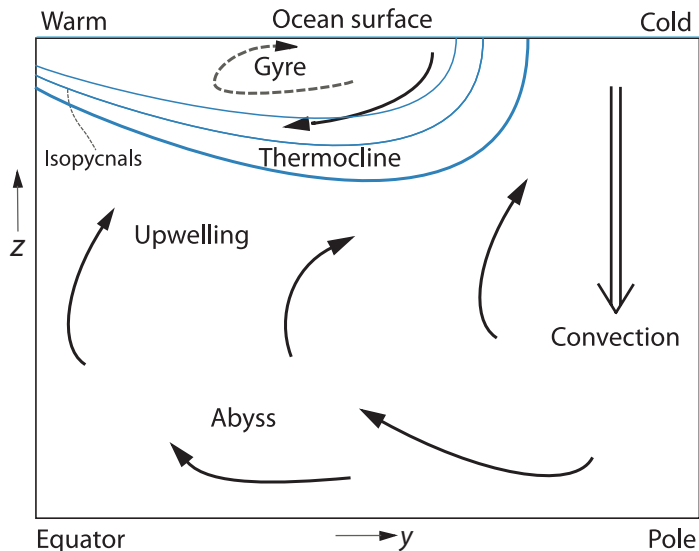


Fig. 20.10 Cartoon of a single-celled meridional overturning circulation, with a wall at the equator.

Sinking is concentrated at high latitudes and upwelling spread out over lower latitudes. The thermocline is the boundary between the cold abyssal waters, with polar origins, and the warmer near-surface subtropical water. Wind forcing in the subtropics pushes the warm surface water into the fluid interior, deepening the thermocline as well as circulating as a gyre.

broadly consistent with this expression. The diffusivity κ can be measured; it is an eddy diffusivity, maintained by small-scale turbulence, and measurements produce values that range between $10^{-5} \text{ m}^2 \text{ s}^{-1}$ in the main thermocline and $10^{-4} \text{ m}^2 \text{ s}^{-1}$ in abyssal regions over rough topography and in and near continental margins, with still higher values locally.⁷ The vertical velocity is too small to be measured directly, but various estimates based on deep water production suggest a value of about 10^{-7} m s^{-1} . Using this and the smaller value of κ in (20.44) gives an e-folding vertical scale, κ/w , of just 100 m, beneath which the stratification is predicted to be very small (i.e., nearly uniform potential density). Using the larger value of κ increases the vertical scale to 1000 m, which is probably closer to the observed value for the total thickness of the thermocline (Fig. 20.9), but using such a large value of κ in the main thermocline is not supported by the observations. Similarly, the deep stratification of the ocean is rather larger than that given by (20.43), except with values of diffusivity on the large side of those observed, a topic we return to in Chapter 21.⁸

Aside from diffusion, mechanical forcing, and in particular the wind, will deepen the thermocline, as Fig. 20.10 suggests. The wind-stress curl forces water to converge in the subtropical Ekman layer, thereby forcing relatively warm water to downwell and meet the upwelling colder abyssal water at some finite depth, thus deepening the thermocline from its purely diffusive value. Indeed, in so far as we can separate the two effects of wind and diffusion, we can say that the strength of the wind influences the *depth* at which the thermocline occurs, whereas the strength of the diffusivity influences the *thickness* of the thermocline.

20.5 SCALING AND SIMPLE DYNAMICS OF THE MAIN THERMOCLINE

We now begin to consider the dynamics that produce an overturning circulation and a thermocline. The Rossby number of the large-scale circulation is small and the scale of the motion large, and the flow obeys the planetary-geostrophic equations,

$$\mathbf{f} \times \mathbf{u} = -\nabla\phi, \quad \frac{\partial\phi}{\partial z} = b, \quad \nabla \cdot \mathbf{v} = 0, \quad \frac{Db}{Dt} = \kappa \frac{\partial^2 b}{\partial z^2}, \quad (20.46a,b,c,d)$$

in our standard notation, in which \mathbf{u} and \mathbf{v} refer to the two- and three-dimensional velocities. We suppose that these equations hold below an Ekman layer, so that the effects of a wind stress may be included by specifying a vertical velocity, w_E , at the top of the domain. The diapycnal diffusivity, κ ,

is some kind of eddy diffusivity, but since its precise form and magnitude are uncertain we proceed with due caution, and a useful practical philosophy is to try to ignore dissipation and viscosity where possible, and to invoke them only if there is no other way out. Let us therefore scale the equations in two ways, with and without diffusion; these scalings will be central to our theory.

20.5.1 A Diffusive Scale

Suppose that the circulation is steady and resembles that of Fig. 20.10, but with no wind forcing. Can we estimate how deep the diffusive layer will be in the subtropical gyre? We will suppose that, as in the kinematic model, the thermodynamic equation reduces to the advective-diffusive balance of (20.43), but we will use the other equations in (20.46) to give an estimate of the vertical velocity. If we take the curl of (i.e., cross differentiate) the momentum equation (20.46a) and use mass continuity we obtain the linear vorticity equation, $\beta v = f \partial w / \partial z$, and if we take the vertical derivative of the momentum equation and use hydrostasy we obtain thermal wind, $\partial \mathbf{u} / \partial z = \mathbf{k} \times \nabla b$. Collecting these equations together we have

$$w \frac{\partial b}{\partial z} = \kappa \frac{\partial^2 b}{\partial z^2}, \quad \beta v = f \frac{\partial w}{\partial z}, \quad f \frac{\partial \mathbf{u}}{\partial z} = \mathbf{k} \times \nabla b, \quad (20.47a,b,c)$$

with corresponding scales

$$\frac{W}{\delta} = \frac{\kappa}{\delta^2}, \quad \beta V = \frac{f W}{\delta}, \quad \frac{U}{\delta} = \frac{\Delta b}{f L}, \quad (20.48a,b,c)$$

where δ is the vertical scale and other scaling values are denoted with capital letters. We suppose that $V \sim U$, where U is the zonal velocity scale, and henceforth we will denote both by U , and L is the horizontal scale of the motion, which we take as the gyre or basin scale. Typical values for the subtropical gyre are $\Delta b = g \Delta \rho / \rho_0 = g \beta_T \Delta T \sim 10^{-2} \text{ m s}^{-2}$, $L = 5000 \text{ km}$, $f = 10^{-4} \text{ s}^{-1}$ and $\kappa = 10^{-5} \text{ m}^2 \text{ s}^{-2}$.

Equation (20.48a) is the same as (20.45), as expected, but we can now use (20.48b,c) to obtain an estimate for the vertical velocity, namely

$$W = \frac{\beta \delta^2 \Delta b}{f^2 L}. \quad (20.49)$$

Using this and (20.48a) gives the diffusive vertical scale, and the estimates

$$\delta = \left(\frac{\kappa f^2 L}{\beta \Delta b} \right)^{1/3}, \quad W = \left(\frac{\kappa^2 \beta \Delta b}{f^2 L} \right)^{1/3}. \quad (20.50)$$

With values of the parameters as above, (20.50) gives $\delta \approx 150 \text{ m}$ and $W \approx 10^{-7} \text{ m s}^{-1}$.

20.5.2 An Advective Scale

The value of the vertical velocity obtained above is very small, much smaller than the Ekman pumping velocity at the top of the ocean, which is of order 10^{-6} – 10^{-5} m s^{-1} . This difference suggests that we might ignore the diffusive term in (20.47a) — indeed, ignore the thermodynamic term completely — and construct an adiabatic scaling estimate for the depth of the wind's influence. Further, in subtropical gyres the Ekman pumping is downward, whereas the diffusive velocity is upward, meaning that at some level, D_a , we expect the vertical velocity to be zero.

The equations of motion are just the thermal wind balance and the linear geostrophic vorticity equation, namely

$$\beta v = f \frac{\partial w}{\partial z}, \quad \mathbf{f} \times \frac{\partial \mathbf{u}}{\partial z} = -\nabla b, \quad (20.51)$$

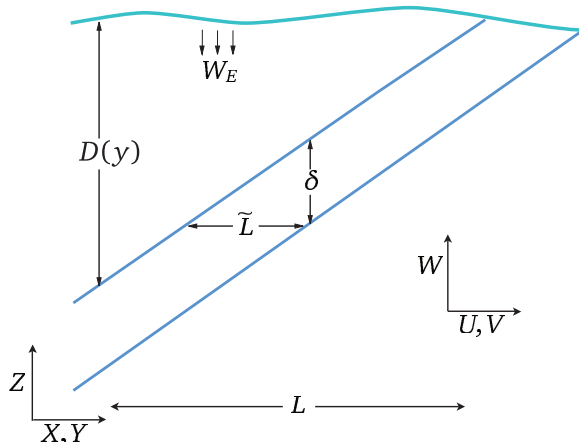


Fig. 20.11 Scaling the thermocline. The diagonal lines mark the diffusive thermocline of thickness δ and depth $D(y)$. The advective scaling for $D(y)$, i.e., D_a , is given by (20.53), and the diffusive scaling for δ is given by (20.55).

with corresponding scales

$$\beta U = f \frac{W}{D_a}, \quad \frac{U}{D_a} = \frac{1}{f} \frac{\Delta b}{L}, \quad (20.52)$$

recalling that $V \sim U$.

The thermodynamic equation does not enter, but we take the vertical velocity to be that due to Ekman pumping, W_E . From (20.52) we immediately obtain

$$D_a = W_E^{1/2} \left(\frac{f^2 L}{\beta \Delta b} \right)^{1/2}, \quad (20.53)$$

which may be compared with the estimate of (20.26). If we relate U and W_E using mass conservation, $U/L = W_E/D_a$, instead of using (20.51a), then we write L in place of f/β and (20.53) becomes $D_a = (W_E f L^2 / \Delta b)^{1/2}$, which is not qualitatively different from (20.53) for large scales.

The important aspect of the above estimate is that the depth of the wind-influenced region increases with the magnitude of the wind stress (because $W_E \propto \text{curl}_z \tau$) and decreases with the meridional temperature gradient. The former dependence is reasonably intuitive, and the latter arises because as the temperature gradient increases the associated thermal wind-shear U/D_a correspondingly increases. But the horizontal transport (the product UD_a) is fixed by mass conservation; the only way that these two can remain consistent is for the vertical scale to decrease. Taking $W_E = 10^{-6} \text{ m s}^{-1}$, and other values as before, gives $D_a = 500 \text{ m}$, and $W_E = 10^{-5} \text{ m s}^{-1}$ gives $D_a = 500 \text{ m}$. Such a scaling argument cannot be expected to give more than an estimate of the depth of the wind-influenced region; nevertheless, because D_a is much less than the ocean depth, the estimate does suggest that the wind-driven circulation is predominantly an upper-ocean phenomenon.

♦ A wind-influenced diffusive scaling

The scalings above assume that the length scale over which thermal wind balance holds is the gyre scale itself. In fact, there is another length scale that is more appropriate, and this leads to a slightly different diffusive scaling for the thickness of the thermocline. To obtain this scaling, we first note that the depth of the subtropical thermocline is not constant: it shoals up to the east because of Sverdrup balance, and it may shoal up polewards as the curl of the wind stress falls (and is zero at the poleward edge of the gyre). Thus, referring to Fig. 20.11, the appropriate horizontal length scale \tilde{L} is given by

$$\tilde{L} = \delta \frac{L}{D_a}. \quad (20.54)$$

This is no longer an externally imposed parameter, but must be determined as part of the solution. Using \tilde{L} instead of L as the length scale in the thermal wind equation (20.48c) gives, using (20.53), the modified diffusive scale

$$\delta = \kappa^{1/2} \left(\frac{f^2 L}{\Delta b \beta D_a} \right)^{1/2} = \kappa^{1/2} \left(\frac{f^2 L}{\Delta b \beta W_E} \right)^{1/4}. \quad (20.55)$$

Substituting values of the various parameters results in a thickness of about 100–200 m. The thermocline thickness now scales as $\kappa^{1/2}$. The interpretation of this scale and that of (20.50) is that the thickness of the thermocline scales as $\kappa^{1/3}$ in the absence of a wind stress, but scales as $\kappa^{1/2}$ if a wind stress is present that can provide a finite slope to the base of the thermocline that is independent of κ , and this is confirmed by numerical simulations.⁹ From (20.47a) the vertical velocity, and hence the meridional overturning circulation, no longer scale as $\kappa^{2/3}$ but as

$$W = \frac{\kappa}{\delta} \propto \kappa^{1/2}. \quad (20.56)$$

20.5.3 Summary of the Physical Picture

What do the vertical scales derived above represent? The wind-influenced scaling, D_a , is the depth to which the directly wind-driven circulation can be expected to penetrate. Thus, over this depth we can expect to see wind-driven gyres and associated phenomena. At greater depths lies the abyssal circulation, and this is not wind-driven in the same sense. Now, in general, the water at the base of the wind-driven layer will not have the same thermodynamic properties as the upwelling abyssal water — this being cold and dense, whereas the water in the wind-driven layer is warm and subtropical (look again at Fig. 20.10). The thickness δ characterizes the diffusive transition region between these two water masses and in the limit of very small diffusivity this becomes a *front*. One might say that D_a is the *depth* of the thermocline, while δ is the *thickness* of the thermocline. In the diffusive region, no matter how small the diffusivity κ is in the thermodynamic equation, the diffusive term is important. Of course if the diffusion is sufficiently large, the thickness will be as large or larger than the depth, and the two regions will blur into each other, and this may indeed be the case in the real ocean. Nevertheless, these scales are a useful foundation on which to build.¹⁰

20.6 THE INTERNAL THERMOCLINE

We now try to go beyond simple scaling arguments and investigate in more detail the dynamics of the thermocline. In this section we consider the diffusive, or internal, thermocline and in Section 20.7 we consider the advective, or ventilated, thermocline. The advective term in the thermodynamic equation makes such an investigation difficult, and prevents us from constructing exact analytic models, but not from constructing informative models. We begin by expressing the planetary-geostrophic equations as an equation in a single unknown.

20.6.1 The M Equation

The planetary-geostrophic equations can be written as a single partial differential equation in a single variable, although the resulting equation is of quite high order and is nonlinear. We write the equations of motion as

$$-fv = -\frac{\partial \phi}{\partial x}, \quad fu = -\frac{\partial \phi}{\partial y}, \quad b = \frac{\partial \phi}{\partial z}, \quad (20.57a,b,c)$$

$$\nabla \cdot \mathbf{v} = 0, \quad \frac{\partial b}{\partial t} + \mathbf{v} \cdot \nabla b = \kappa \nabla^2 b, \quad (20.58a,b)$$

where we take $f = \beta y$. Cross-differentiating the horizontal momentum equations and using (20.58a) gives the linear geostrophic vorticity relation $\beta v = f \partial w / \partial z$ which, using (20.57a) again, may be written as

$$\frac{\partial \phi}{\partial x} + \frac{\partial}{\partial z} \left(-\frac{f^2}{\beta} w \right) = 0. \quad (20.59)$$

This equation is the divergence in (x, z) of $(\phi, -f^2 w / \beta)$ and is automatically satisfied if

$$\phi = M_z \quad \text{and} \quad \frac{f^2 w}{\beta} = M_x, \quad (20.60a,b)$$

where the subscripts on M denote derivatives. Then straightforwardly

$$u = -\frac{\partial_y \phi}{f} = -\frac{M_{zy}}{f}, \quad v = \frac{\partial_x \phi}{f} = \frac{M_{zx}}{f}, \quad b = \partial_z \phi = M_{zz}. \quad (20.61a,b,c)$$

The thermodynamic equation, (20.58b) becomes

$$\frac{\partial M_{zz}}{\partial t} + \left(\frac{-M_{zy}}{f} M_{zzx} + \frac{M_{zx}}{f} M_{zzy} \right) + \frac{\beta}{f^2} M_x M_{zzz} = \kappa M_{zzzz} \quad (20.62)$$

or

$$\frac{\partial M_{zz}}{\partial t} + \frac{1}{f} J(M_z, M_{zz}) + \frac{\beta}{f^2} M_x M_{zzz} = \kappa M_{zzzz}, \quad (20.63)$$

where J is the usual horizontal Jacobian. This is the M equation,¹¹ somewhat analogous to the potential vorticity equation in quasi-geostrophic theory in that it expresses the entire dynamics of the system in a single, nonlinear, advective–diffusive partial differential equation, although M_{zz} is materially conserved (in the absence of diabatic effects) by the three-dimensional flow. Because of the high differential order and nonlinearity of the system, analytic solutions of (20.63) are hard to find, and from a numerical perspective it is easier to integrate the equations in the form (20.57) and (20.58) than in the form (20.63). Nevertheless, it is possible to move forward by approximating (20.63) to one or two dimensions, or by a priori assuming a boundary-layer structure.

A one-dimensional model

Let us consider an illustrative one-dimensional model (in z) of the thermocline.¹² Merely setting all horizontal derivatives in (20.63) to zero is not very useful, for then all the advective terms on the left-hand side vanish. Rather, we look for steady solutions of the form $M = M(x, z)$, and the M equation then becomes

$$\frac{\beta}{f^2} M_x M_{zzz} = \kappa M_{zzzz}, \quad (20.64)$$

which represents the advective–diffusive balance

$$w \frac{\partial b}{\partial z} = \kappa \frac{\partial^2 b}{\partial z^2}. \quad (20.65)$$

In proceeding in this way we have assumed that the value of κ varies meridionally in the same manner as does β/f^2 ; without this technicality M would be a function of y , violating our premise.

If the ocean surface is warm and the abyss is cold, then (20.64) represents a balance between the upward advection of cold water and the downward diffusion of warm water. The horizontal

advection terms vanish because the zonal velocity, u , and the meridional buoyancy gradient, b_y , are each zero. Let us further consider the special case

$$M = (x - x_e)W(z), \quad (20.66)$$

where the domain extends from $0 \leq x \leq x_e$, so satisfying $M = 0$ on the eastern boundary. Equation (20.64) becomes the ordinary differential equation

$$\frac{\beta}{f^2} WW_{zzz} = \kappa W_{zzzz}, \quad (20.67)$$

where W has the dimensions of velocity squared. We nondimensionalize this by setting

$$z = H\hat{z}, \quad \kappa = \hat{\kappa}(HW_S), \quad W = \left(\frac{f^2 W_S}{\beta} \right) \hat{W}, \quad (20.68a,b,c)$$

where the hatted variables are nondimensional and W_S is a scaling value of the dimensional vertical velocity, w (e.g., the magnitude of the Ekman pumping velocity W_E). Equation (20.67) becomes

$$\hat{W}\hat{W}_{\hat{z}\hat{z}\hat{z}} = \hat{\kappa}\hat{W}_{\hat{z}\hat{z}\hat{z}\hat{z}}. \quad (20.69)$$

The parameter $\hat{\kappa}$ is a nondimensional measure of the strength of diffusion in the interior, and the interesting case occurs when $\hat{\kappa} \ll 1$; in the ocean, typical values are $H = 1$ km, $\kappa = 10^{-5}$ m s⁻² and $W_S = W_E = 10^{-6}$ m s⁻¹ so that $\hat{\kappa} \approx 10^{-2}$, which is indeed small. (It might appear that we could completely scale away the value of κ in (20.67) by scaling W appropriately, and if so there would be no meaningful way that one could say that κ was small. However, this is a chimera, because the value of κ would still appear in the boundary conditions.)

The time-dependent form of (20.69), namely $\hat{W}_{\hat{z}\hat{z}t} + \hat{W}\hat{W}_{\hat{z}\hat{z}\hat{z}} = \hat{\kappa}\hat{W}_{\hat{z}\hat{z}\hat{z}\hat{z}}$, is similar to Burger's equation, $V_t + VV_z = \nu V_{zz}$, which is known to develop fronts. (In the inviscid Burger's equation, $DV/Dt = 0$, where the advective derivative is one-dimensional, and therefore the velocity of a given fluid parcel is preserved on the line. Suppose that the velocity of the fluid is positive but diminishes in the positive z -direction, so that a fluid parcel will catch-up with the fluid parcel in front of it. But since the velocity of a fluid parcel is fixed, there are two values of velocity at the same point, so a singularity must form. In the presence of viscosity, the singularity is tamed to a front.) Thus, we might similarly expect (20.69) to produce a front, but because of the extra derivatives the argument is not as straightforward and it is simplest to obtain solutions numerically.

Equation (20.69) is fourth order, so four boundary conditions are needed, two at each boundary. Appropriate ones are a prescribed buoyancy and a prescribed vertical velocity at each boundary, for example

$$\begin{aligned} \hat{W} &= \hat{W}_E, & -\hat{W}_{\hat{z}\hat{z}} &= B_0, & \text{at top,} \\ \hat{W} &= 0, & -\hat{W}_{\hat{z}\hat{z}} &= 0, & \text{at bottom,} \end{aligned} \quad (20.70)$$

where \hat{W}_E is the (nondimensional) vertical velocity at the base of the top Ekman layer, which is negative for Ekman pumping in the subtropical gyre, and B_0 is a constant, proportional to the buoyancy difference across the domain. We obtain solutions numerically by Newton's method,¹³ and these are shown in Figs. 20.12 and 20.13. The solutions do indeed display fronts, or boundary layers, for small diffusivity. If the wind forcing is zero (Fig. 20.13), the boundary layer is at the top of the fluid. If the wind forcing is non-zero, an internal boundary layer — a front — forms in the fluid interior with an adiabatic layer above and below. In the real ocean, where wind forcing is of course non-zero, the frontal region is known as the *internal thermocline*.

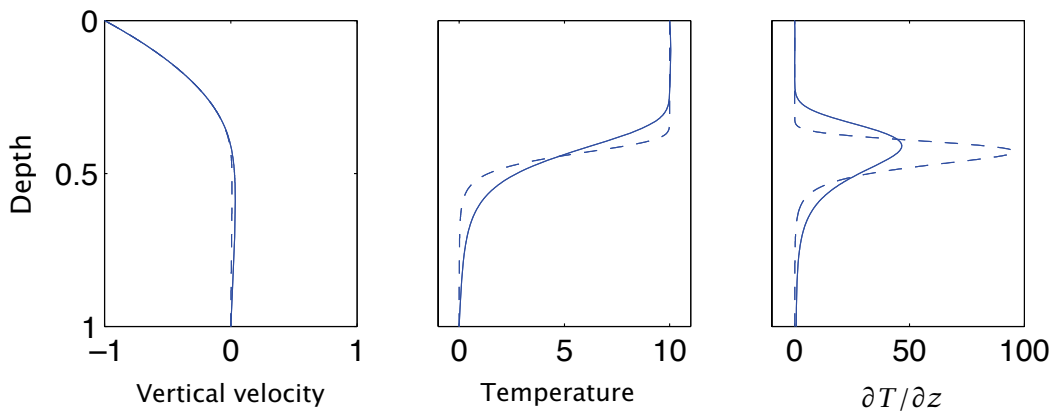


Fig. 20.12 Solution of the one-dimensional thermocline equation, (20.69), with boundary conditions (20.70), for two different values of the diffusivity: $\hat{\kappa} = 3.2 \times 10^{-3}$ (solid line) and $\hat{\kappa} = 0.4 \times 10^{-3}$ (dashed line), in the domain $0 \leq \hat{z} \leq -1$. ‘Vertical velocity’ is W , ‘temperature’ is $-W_{\hat{z}\hat{z}}$, and all units are the nondimensional ones of the equation itself. A negative vertical velocity, $\hat{W}_E = -1$, is imposed at the surface (representing Ekman pumping) and $B_0 = 10$.

The internal boundary layer thickness increases as $\hat{\kappa}^{1/3}$, so doubling in thickness for an eightfold increase in $\hat{\kappa}$. The upwelling velocity also increases with $\hat{\kappa}$ (as $\hat{\kappa}^{2/3}$), but this is barely noticeable on the graph because the downwelling velocity, above the internal boundary layer, is much larger and almost independent of $\hat{\kappa}$. The depth of the boundary layer increases as $\hat{W}_E^{1/2}$, so if $\hat{W}_E = 0$ the boundary layer is at the surface, as in Fig. 20.13.

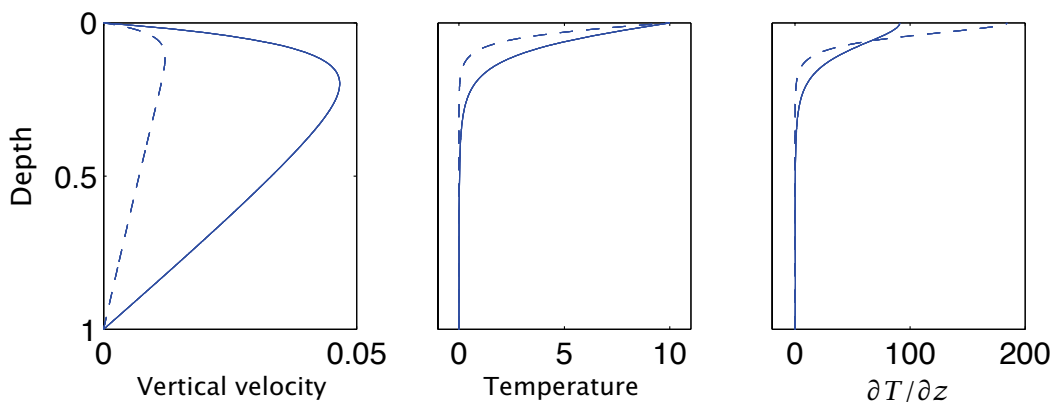


Fig. 20.13 As for Fig. 20.12, but with no imposed Ekman pumping velocity at the upper boundary ($\hat{W}_E = 0$), again for two different values of the diffusivity: $\hat{\kappa} = 3.2 \times 10^{-3}$ (solid line) and $\hat{\kappa} = 0.4 \times 10^{-3}$ (dashed line). The boundary layer now forms at the upper surface. The boundary thickness again increases with diffusivity and, even more noticeably, so does the upwelling velocity — this scales as $\hat{\kappa}^{2/3}$, and so increases fourfold for an eightfold increase in $\hat{\kappa}$.

20.6.2 ♦ Boundary-layer Analysis

The reasoning and the numerical solutions of the above sections suggest that the internal thermocline has a boundary-layer structure whose thickness decreases with κ . If the Ekman pumping at the top of the ocean is non-zero, the boundary layer is internal to the fluid. To learn more, let us perform a boundary layer analysis, much as we did when investigating western boundary currents in Section 19.1.3. The nonlinearity precludes a complete solution of the equation, but we can

nevertheless obtain some useful information.

One-dimensional model

Let us now *assume* a steady two-layer structure of the form illustrated in Fig. 20.14, and that the dynamics are governed by (20.69) in a domain that extends from 0 to -1 . The buoyancy thus varies rapidly only in an internal boundary layer of nondimensional thickness $\hat{\delta}$ located at $\hat{z} = -h$; above and below this the buoyancy is assumed to be only very slowly varying. Following standard boundary layer procedure we introduce a stretched boundary layer coordinate ζ where

$$\hat{\delta}\zeta = \hat{z} + h. \quad (20.71)$$

That is, ζ is the distance from $\hat{z} = -h$, scaled by the boundary layer thickness $\hat{\delta}$, and within the boundary layer ζ is an order-one quantity. We also let

$$\widehat{W}(\hat{z}) = \widehat{W}_I(\hat{z}) + \widetilde{W}(\zeta), \quad (20.72)$$

where \widehat{W}_I is the solution away from the boundary layer and \widetilde{W} is the boundary layer correction. Because the boundary layer is presumptively thin, \widehat{W}_I is effectively constant through it and, furthermore, for $\hat{z} < -h$, \widetilde{W} vanishes in the limit as $\kappa = 0$. We thus take $\widehat{W}_I = 0$ throughout the boundary layer. (The small diffusively-driven upwelling below the boundary layer is part of the boundary layer solution, not the interior solution.) Now, buoyancy varies rapidly in the boundary layer but it remains an order-one quantity throughout. To satisfy this we explicitly scale \widetilde{W} in the boundary layer by writing

$$\widetilde{W}(\zeta) = \hat{\delta}^2 B_0 A(\zeta), \quad (20.73)$$

where B_0 is defined by (20.70) and A is an order-one field. The derivatives of W are

$$\frac{\partial \widehat{W}}{\partial \hat{z}} = \frac{1}{\hat{\delta}} \frac{\partial \widetilde{W}}{\partial \zeta} = \hat{\delta} B_0 \frac{\partial A}{\partial \zeta}, \quad \frac{\partial^2 \widehat{W}}{\partial \hat{z}^2} = B_0 \frac{\partial^2 A}{\partial \zeta^2}, \quad (20.74)$$

so that $\widehat{W}_{\hat{z}\hat{z}}$ is an order-one quantity. Far from the boundary layer the solution must be able to match the external conditions on temperature and velocity, (20.70); the buoyancy condition on $W_{\hat{z}\hat{z}}$ is satisfied if

$$A_{\zeta\zeta} \rightarrow \begin{cases} 1 & \text{as } \zeta \rightarrow +\infty \\ 0 & \text{as } \zeta \rightarrow -\infty. \end{cases} \quad (20.75)$$

On vertical velocity we require that $W \rightarrow (\hat{z}/h+1)W_E$ as $\zeta \rightarrow +\infty$, and $W \rightarrow \text{constant}$ as $\zeta \rightarrow -\infty$. The first matches the Ekman pumping velocity above the boundary layer, and the second condition produces the abyssal upwelling velocity, which as noted vanishes for $\kappa \rightarrow 0$.

Substituting (20.72) and (20.73) into (20.69) we obtain

$$B_0 A A_{\zeta\zeta\zeta} = \frac{\hat{\kappa}}{\hat{\delta}^3} A_{\zeta\zeta\zeta\zeta}. \quad (20.76)$$

Because all quantities are presumptively $\mathcal{O}(1)$, (20.76) implies that $\hat{\delta} \sim (\hat{\kappa}/B_0)^{1/3}$. We restore the dimensions of δ by using $\kappa = \hat{\kappa}(HW_S)$ and $\Delta b = B_0 L f^2 W_S / (\beta H^2)$, where Δb is the dimensional buoyancy difference across the boundary layer — note that $b = M_{zz} = (x-1)W_{zz} \sim LW_{zz} \sim LB_0 f^2 W_S / (\beta H^2)$ using (20.68). The dimensional boundary layer thickness, δ , is then given by

$$\delta \sim \left(\frac{\kappa f^2 L}{\Delta b \beta} \right)^{1/3}, \quad (20.77)$$

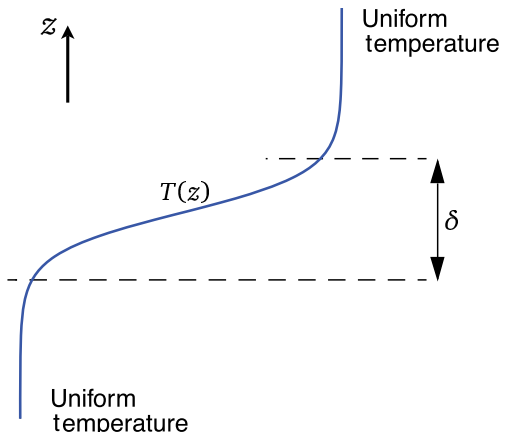


Fig. 20.14 The simplified boundary-layer structure of the internal thermocline. In the limit of small diffusivity the internal thermocline forms a boundary layer, of thickness δ in the figure, in which the temperature and buoyancy change rapidly.

which is the same as the heuristic estimate (20.50). The dimensional vertical velocity scales as

$$W \sim \frac{\kappa}{\delta} \sim \kappa^{2/3} \left(\frac{\Delta b \beta}{f^2 L} \right)^{1/3}, \quad (20.78)$$

this being an estimate of strength of the upwelling velocity at the base of the thermocline and, more generally, the strength of the diffusively-driven component of meridional overturning circulation of the ocean.

Although the detailed properties of such one-dimensional thermocline models depend on the details of model construction, two significant features are robust:

- (i) The thickness of the internal thermocline increases with increasing diffusivity, and decreases with increasing buoyancy difference across it, and as the diffusivity tends to zero the thickness of the internal thermocline tends to zero.
- (ii) The strength of the upwelling velocity, and hence the strength of the meridional overturning circulation, increase with increasing diffusivity and increasing buoyancy difference.

♦ *The three-dimensional equations*

We now apply boundary layer techniques to the three-dimensional M equation.¹⁴ The main difference is that the depth of the boundary layer is now a function of x and y , so that the stretched coordinate ζ is given by

$$\widehat{\delta}\zeta = z + h(x, y). \quad (20.79)$$

(The coordinates (x, y, z) in this subsection are nondimensional, but we omit their hats to avoid too cluttered a notation.) Just as in the one-dimensional case we rescale M in the boundary layer and write

$$M = B_0 \widehat{\delta}^2 \widehat{A}(x, y, \zeta), \quad (20.80)$$

where the scaling factor $\widehat{\delta}^2$ again ensures that the temperature remains an order-one quantity. In the boundary layer the derivatives of M become

$$\frac{\partial M}{\partial z} = \frac{1}{\widehat{\delta}} \frac{\partial A}{\partial \zeta}, \quad (20.81)$$

and

$$\frac{\partial M}{\partial x} = \widehat{\delta}^2 B_0 \left(\frac{\partial A}{\partial \zeta} \frac{\partial \zeta}{\partial x} + \frac{\partial A}{\partial x} \right) = \widehat{\delta}^2 B_0 \left(\frac{\partial A}{\partial \zeta} \frac{1}{\widehat{\delta}} \frac{\partial h}{\partial x} + \frac{\partial A}{\partial x} \right). \quad (20.82)$$

Substituting these into (20.62) we obtain, omitting the time-derivative,

$$\begin{aligned} \hat{\delta} \left[\frac{1}{f} (A_{\zeta x} A_{\zeta \zeta y} - A_{\zeta y} A_{\zeta \zeta x}) + \frac{\beta}{f^2} A_x A_{\zeta \zeta \zeta} \right] + \frac{\beta}{f^2} h_x A_\zeta A_{\zeta \zeta \zeta} \\ + \frac{1}{f} [h_x (A_{\zeta \zeta} A_{\zeta \zeta y} - A_{\zeta y} A_{\zeta \zeta \zeta}) + h_y (A_{\zeta x} A_{\zeta \zeta \zeta} - A_{\zeta \zeta} A_{\zeta \zeta x})] = \frac{\kappa}{B_0 \hat{\delta}^2} A_{\zeta \zeta \zeta}, \end{aligned} \quad (20.83)$$

where the subscripts on A and h denote derivatives. If $h_x = h_y = 0$, that is if the base of the thermocline is flat, then (20.83) becomes

$$\frac{1}{f} [A_{\zeta x} A_{\zeta \zeta y} - A_{\zeta y} A_{\zeta \zeta x}] + \frac{\beta}{f^2} A_x A_{\zeta \zeta \zeta} = \frac{\kappa}{B_0 \hat{\delta}^3} A_{\zeta \zeta \zeta}. \quad (20.84)$$

Since all the terms in this equation are, by construction, order one, we immediately see that the nondimensional boundary layer thickness $\hat{\delta}$ scales as

$$\hat{\delta} \sim \left(\frac{\kappa}{B_0} \right)^{1/3}, \quad (20.85)$$

just as in the one-dimensional model. On the other hand, if h_x and h_y are order-one quantities then the dominant balance in (20.83) is

$$\frac{1}{f} [h_x (A_{\zeta \zeta} A_{\zeta \zeta y} - A_{\zeta y} A_{\zeta \zeta \zeta}) + h_y (A_{\zeta x} A_{\zeta \zeta \zeta} - A_{\zeta \zeta} A_{\zeta \zeta x})] = \frac{\kappa}{B_0 \hat{\delta}^2} A_{\zeta \zeta \zeta} \quad (20.86)$$

and

$$\hat{\delta} \sim \left(\frac{\kappa}{B_0} \right)^{1/2}, \quad (20.87)$$

confirming the heuristic scaling arguments. Thus, if the isotherm slopes are fixed independently of κ (for example, by the wind stress), then as $\kappa \rightarrow 0$ an internal boundary layer will form whose thickness is proportional to $\kappa^{1/2}$. We expect this to occur at the base of the main thermocline, with purely advective dynamics being dominant in the upper part of the thermocline, and determining the slope of the isotherms (i.e., the form of h_x and h_y), as in Fig. 20.11. Interestingly, the balance in the three-dimensional boundary layer equation does not in general correspond locally to $wT_z \approx \kappa T_{zz}$. Both at $\mathcal{O}(1)$ and $\mathcal{O}(\delta)$ the horizontal advective terms in (20.83) are of the same asymptotic size as the vertical advection terms. In the boundary layer the thermodynamic balance is thus $\mathbf{u} \cdot \nabla_z T + wT_z \approx \kappa T_{zz}$, whether the isotherms are sloping or flat. We might have anticipated this, because the vertical velocity passes through zero within the boundary layer.

What are the dynamics above the diffusive layer, presuming that it does not extend all the way to the surface? Answering this leads us into our next topic, the ‘ventilated thermocline’.

20.7 THE VENTILATED THERMOCLINE

We now consider the nature of the dynamics *above* the diffusive layer, presuming that the diffusivity is sufficiently small that there is a meaningful separation of the internal boundary layer and the advective dynamics above. In the advective region there is no general reason that the temperature profile should be uniform, and we envision an essentially adiabatic region that is both wind-driven and stratified. This region of the thermocline has become known, for reasons that will become apparent, as the *ventilated thermocline*. The main thermocline is composed of the internal thermocline plus a ventilated region, and to set our bearings it may be useful to refer now to the overall picture sketched in Fig. 20.15 and the shaded box on page 790.

To elucidate the structure of the ventilated thermocline we will assume the following:¹⁵

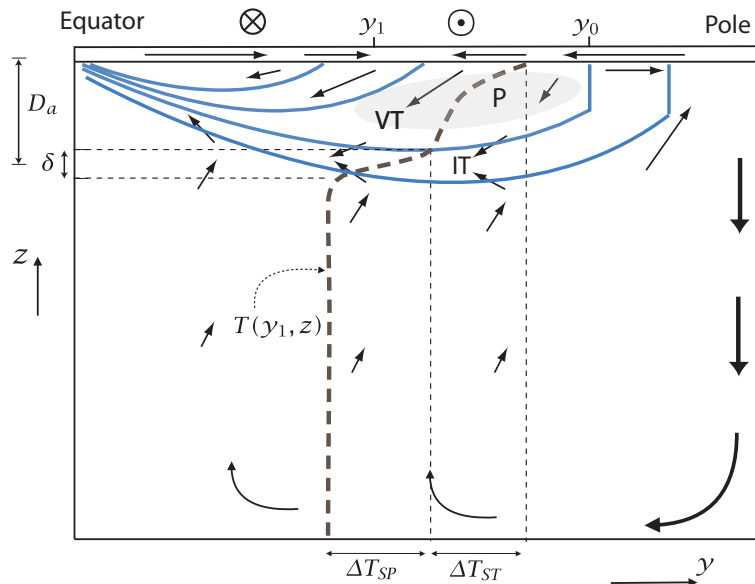


Fig. 20.15 Idealization of the large-scale circulation and structure of the main thermocline, in a single-hemisphere ocean driven by wind stress (\odot and \otimes) and a surface temperature that decreases monotonically from equator to pole.

The thin arrows indicate the meridional overturning circulation and the flow in the Ekman layer near the ocean surface. The thick dashed line is a temperature profile, $T(y_1, z)$ at the subtropical latitude y_1 , where the horizontal axis is temperature. The solid blue lines are isotherms and the homogenized western pool region is shaded grey.

Key: VT – ventilated thermocline. IT – internal thermocline. P – pool region in west. δ – thickness of the internal thermocline. D_a – depth of the ventilated thermocline. ΔT_{ST} – temperature drop across subtropical gyre and across ventilated thermocline. ΔT_{SP} – temperature drop across the subpolar gyre and internal thermocline. y_0 – subtropical-subpolar gyre boundary. y_1 – a latitude in the subtropical gyre.

- The motion satisfies the ideal, steady, planetary-geostrophic equations.
- The surface temperature, and the vertical velocity due to Ekman pumping, are given. (These surface conditions are, in reality, influenced by the ocean's dynamics, but we assume that we can calculate a solution with specified surface conditions.) At the base of the wind-influenced region we will impose $w = 0$.
- Rather than use the continuously stratified equations, we will assume that the solution can be adequately represented by a small number of layers, each of constant density. The abyss is represented by a single stationary layer.
- We will not take into account the possible effects of a western boundary current. In that sense the model is an extension of the Sverdrup interior of homogeneous models.

The model is thus not a complete one, yet we may hope that it is revealing about the structure of the real ocean.

20.7.1 A Reduced Gravity, Single-layer Model

The simplest possible model along these lines is to suppose the ocean is composed of just two layers, and only one moving layer, as illustrated in Fig. 20.16. The upper layer of density ρ_1 is wind-driven, whereas the lower layer of density ρ_2 is assumed to be stationary; this is called a ‘one-and-a-half-layer’ model or a ‘reduced gravity single-layer’ model. Pertinent questions are, how deep is the upper layer? What is the velocity field in it?

In the planetary-geostrophic approximation, the momentum and mass conservation equations

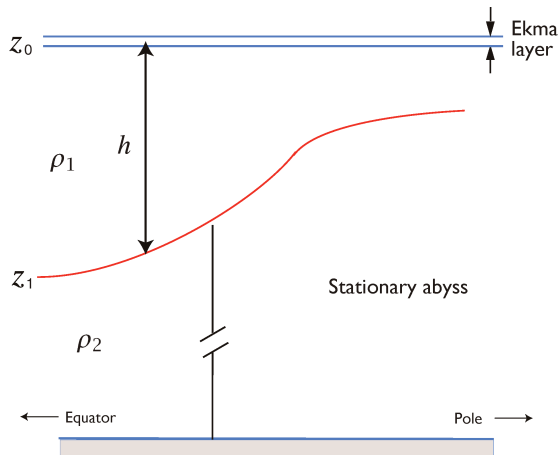


Fig. 20.16 A reduced gravity, single-layer model. A single moving layer lies above a deep, stationary layer of higher density. The upper surface is rigid. A thin Ekman layer may be envisioned to lie on top of the moving layer, providing a vertical velocity boundary condition.

of the reduced gravity shallow water model may be written as:

$$\mathbf{f} \times \mathbf{u} = -g' \nabla h, \quad \nabla \cdot \mathbf{u} = -\frac{\partial w}{\partial z}, \quad (20.88a,b)$$

where ∇ is a two-dimensional operator (as it will be for the rest of this section) and $g' = g(\rho_2 - \rho_1)/\rho_0$ is the *reduced gravity*. Taking the curl of (20.88a) gives the geostrophic vorticity equation, $\beta v + f \nabla \cdot \mathbf{u} = 0$, and integrating this over the depth of the layer and using mass conservation gives

$$h\beta v = f(w_E - w_b), \quad (20.89)$$

where w_E is the velocity at the top of the layer, due mainly to Ekman pumping, and w_b is the vertical velocity at the layer base. If the flow is steady, w_b is zero for then

$$w_b = \mathbf{u} \cdot \nabla h = -\frac{g'}{f} \frac{\partial h}{\partial y} \frac{\partial h}{\partial x} + \frac{g'}{f} \frac{\partial h}{\partial x} \frac{\partial h}{\partial y} = 0. \quad (20.90)$$

Using this result and geostrophic balance, (20.89) becomes

$$\frac{g'}{f} \beta h \frac{\partial h}{\partial x} = f w_E, \quad (20.91)$$

which integrates to

$$h^2 = -2 \frac{f^2}{g' \beta} \int_x^{x_e} w_E dx' + H_e^2, \quad (20.92)$$

where H_e is the (unknown) value of h at the eastern boundary x_e , and it is a constant to satisfy the no-normal flow condition. This apart, the equation contains complete information about the solution. We note that:

- the depth of the moving layer scales as the magnitude of the wind stress (or Ekman pumping velocity) to the one-half power;
- the horizontal solution is similar to the simpler Sverdrup interior solution previously obtained in Section 19.1.3;
- there is no solution if w_E is positive; that is, if there is Ekman upwelling;
- the solution depends on the unknown parameter H_e , the layer depth at the eastern boundary. (That the eastern boundary depth is undetermined is perhaps the main incomplete aspect of the theory as presented here.¹⁶)

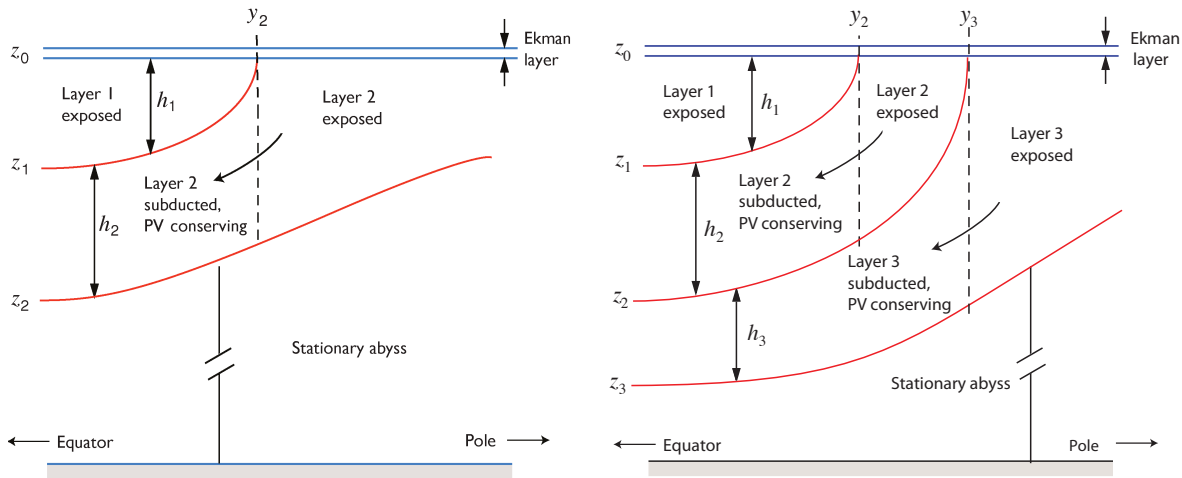


Fig. 20.17 Two-layer (left) and three-layer (right) schematics of the ventilated thermocline, each with a stationary abyss. Models with still more moving layers may be constructed, at least in principle, by extension.

20.7.2 Two-layer and Three-layer Models

Imagine now there are two moving layers above a stationary abyss, as in Fig. 20.17. If there is a meridional buoyancy gradient at the surface then isopycnals *outcrop*, or intersect the surface. Thus, at some latitude (say $y = y_2$, which for simplicity we assume not to be a function of longitude) layer 2 passes underneath layer 1, which is of lower density, as sketched in Fig. 20.17.

Thus, polewards of y_2 the dynamics are just those of a single layer discussed above, whereas equatorward of y_2 layer 2 does not feel the wind directly, and its dynamics are governed by two principles:

- (i) Sverdrup balance. This still applies to the vertically integrated motion, and thus to the sum of layer 1 and layer 2.
- (ii) Conservation of potential vorticity. The motion in layer 2 is shielded from the wind forcing, and the effects of dissipation are assumed to be negligible. Thus, the fluid parcels in the layer will conserve their potential vorticity.

We first use potential vorticity conservation to obtain an expression for the depth of each layer in terms of the total depth of the moving fluid, h , and then use Sverdrup balance to obtain h .

We can apply exactly the same procedure if there are three (or more) moving layers, as in the right-hand panel of Fig. 20.17, and in principle go to the limit of continuous stratification. However, the algebra becomes considerably more complicated and most of the essential dynamics are contained in two layers, so that is our focus.

Potential vorticity conservation

Conservation of potential vorticity in the region equatorward of y_2 is, for steady flow,

$$\mathbf{u}_2 \cdot \nabla q_2 = 0 \quad \text{for} \quad y < y_2, \quad (20.93)$$

where $q_2 = f/h_2$. Now, the velocity field in layer 2 is given by $\mathbf{u}_2 = (g'_2/f)\mathbf{k} \times \nabla h$, where $h = h_1 + h_2$ is the total depth of the moving fluid (see the appendix to this chapter). Thus, (20.93) becomes

$$-\frac{g'_2}{f} \frac{\partial h}{\partial y} \frac{\partial}{\partial x} \left(\frac{f}{h_2} \right) + \frac{g'_2}{f} \frac{\partial h}{\partial x} \frac{\partial}{\partial y} \left(\frac{f}{h_2} \right) = \frac{g'_2}{f} J \left(\frac{f}{h_2}, h \right) = 0. \quad (20.94)$$

This is an equation relating h and h_2 and it has the general solution

$$q_2 \equiv \frac{f}{h_2} = G_2(h), \quad (20.95)$$

where G_2 is an *arbitrary* function of its argument. However, we *know* what the potential vorticity of layer 2 is at the moment it is subducted; it is just

$$q_2(y_2) \equiv \frac{f(y_2)}{h_2} = \frac{f_2}{h}, \quad (20.96)$$

where $f_2 \equiv f(y_2)$, and $h_2 = h$ because $h_1 = 0$. This relationship must therefore hold everywhere in layer 2, equatorwards of y_2 ; that is,

$$G_2(h) = \frac{f_2}{h}. \quad (20.97)$$

Thus, in the subducted region, and taking $z_0 = 0$,

$$\frac{f}{h_2} = \frac{f_2}{h} \quad \text{or} \quad \frac{f}{z_1 - z_2} = -\frac{f_2}{z_2}. \quad (20.98)$$

From this we easily obtain expressions for the depth of each layer as a function of the total depth, h , namely

$$h_2 = z_1 - z_2 = \frac{f}{f_2}h \quad \text{and} \quad h_1 = -z_1 = \left(1 - \frac{f}{f_2}\right)h. \quad (20.99)$$

It remains only to find an expression for the total depth of the moving fluid, h , and this we do using Sverdrup balance. Note that because potential vorticity, f/h_2 , is conserved, as the subducted fluid column moves equatorward its thickness must decrease.

Using Sverdrup balance to find the total depth

Equations (20.99) contain the unknown total depth h , and we now use Sverdrup balance to find this and close the problem. The linear vorticity equation is $\beta v = f \partial w / \partial z$, where the velocity at the top of layer one is that due to the Ekman layer and the velocity at the base of layer two is zero. Given this, we may write the Sverdrup balance as

$$\beta(h_1 v_1 + h_2 v_2) = f w_E, \quad (20.100)$$

where, using (20.128), the velocities in each layer are given by

$$f v_1 = \frac{\partial}{\partial x} (g'_2 h + g'_1 h_1) \quad \text{and} \quad f v_2 = \frac{\partial}{\partial x} (g'_2 h). \quad (20.101)$$

Using these, Sverdrup balance becomes

$$\beta h_1 \frac{\partial}{\partial x} (g'_2 h + g'_1 h_1) + \beta(h - h_1) g'_2 \frac{\partial h}{\partial x} = f^2 w_E, \quad (20.102)$$

or

$$\frac{\partial}{\partial x} (g'_2 h^2 + g'_1 h_1^2) = \frac{2f^2}{\beta} w_E. \quad (20.103)$$

On integrating, the above equation becomes

$$\left(h^2 + \frac{g'_1}{g'_2} h_1^2\right) = D_0^2 + C, \quad \text{where} \quad D_0^2(x, y) = -\frac{2f^2}{\beta g'_2} \int_x^{x_e} w_E(x', y) dx', \quad (20.104a,b)$$

Thermocline Dynamics — an Overview

The model of the main thermocline that we have constructed in sections 20.4–20.7 is illustrated schematically in Fig. 20.15. Some of the features, and limitations, of this model are listed below:

- The main subtropical thermocline consists of an advective upper region overlying a diffusive base.
 - The diffusive base forms the *internal thermocline*, and in the limit of small diffusivity this is an internal boundary layer. The advective region forms the *ventilated thermocline*. The separation of the two regions may, in reality, not be sharp.
 - The relative thickness of these layers is a function of various parameters, notably the strength of the wind and the magnitude of the diffusivity.
 - Above the ventilated thermocline there may be a mixed layer with a seasonally varying depth. In certain regions, for example at the poleward edge of the subtropical gyre, convection may deepen the mixed layer as far as the base of the thermocline.
 - In the thermocline theories we have presented there is no explicit western boundary layer. Such a boundary layer is needed to close the circulation and the heat budget.
 - The single-hemisphere model assumes that the water that sinks at high latitude either upwells through the main thermocline or returns to the subpolar gyre beneath the main thermocline. In reality some of this water may cross into the other hemisphere before upwelling — more so in the Atlantic than Pacific.
 - In this case, the diffusion-dependent overturning circulation represents only part of the overall meridional overturning circulation.
 - Nevertheless, there would remain a diffusive internal thermocline (and a ventilated thermocline above it) because there is still a boundary between the warm subtropical water and cold abyssal water.
 - Within the ventilated thermocline there are two regions — the shadow zone and the western pool — whose dynamics are not determined without additional assumptions. Plausible assumptions for the western pool are:
 - All the water within it is ventilated, leading to a model of mode water.
 - The potential vorticity within the pool is homogenized through the action of mesoscale eddies.
- Some combination of these might also apply. The size of the pool region increases as the poleward boundary of the pool region approaches the latitude of the outcrop (Fig. 20.21) and can extend almost across the entire gyre.
- Topics of research include questions of how potential vorticity homogenization is affected by a western boundary current, if and how the non-passive nature of potential vorticity affects the pool region, and if and how all these concepts apply in the real ocean.

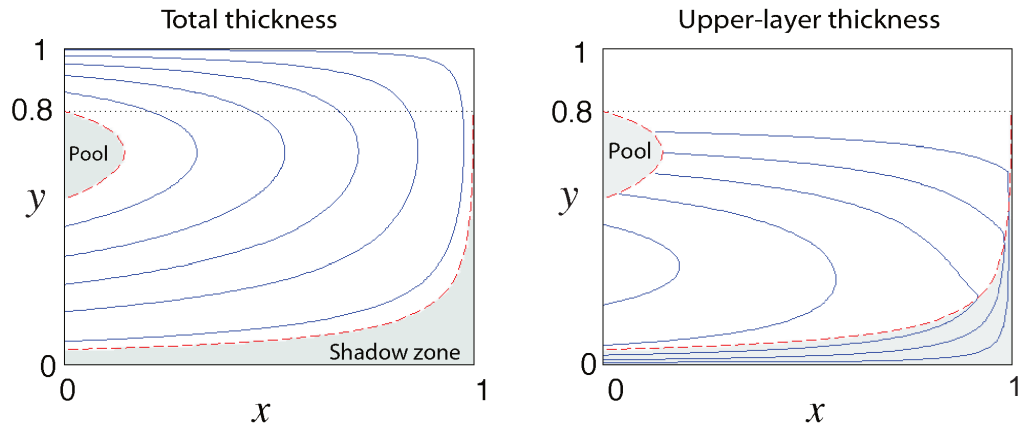


Fig. 20.18 Contour plots of total thickness and upper layer thickness in a two-layer model of the ventilated thermocline. The thickness generally increases westwards, and the flow is clockwise. The shadow zone and the western pool are shaded, and no contours are drawn in the latter. The outcrop latitude, $y_2 = 0.8$, is marked with a dotted line. The parameters used are $g'_1 = g'_2 = 1$, $\beta = 1$, $f_0 = 0.5$, $H_e = 0.5$, and $w_E = -\sin(\pi y)$.

which by construction vanishes at the eastern wall ($x = x_e$). The constant of integration C may be interpreted as follows. Let us write $C = H_e^2 + (g'_1/g'_2)H_1^2$ where H_e is the (unknown) total depth of layers 1 and 2 at the eastern boundary, and H_1 is the depth of layer 1. These must both be constants in order to satisfy the no-normal flow condition. However, H_1 must be zero, because at the outcrop line $h_1 = 0$. Thus, H_1 is zero at $y = y_2$, and therefore zero everywhere, and $C = H_e^2$.

Using (20.99) and (20.104) we obtain a closed expression for h , namely

$$h = -z_2 = \frac{(D_0^2 + H_e^2)^{1/2}}{[1 + (g'_1/g'_2)(1 - f/f_2)^2]^{1/2}}. \quad (20.105)$$

Using (20.99) the depths in each layer, and the corresponding geostrophic velocities, can readily be obtained.

A typical solution is shown in Fig. 20.18. The upper layer exists only equatorward of the outcrop latitude, $y_2 = 0.8$, and isolines of total thickness correspond to streamlines of the lower layer. We see, as expected, the overall shape of a subtropical gyre, with the circulation being closed by an implicit western boundary current that is not part of the calculation. Two regions are shaded in the figure, the ‘pool’ region in the west and the ‘shadow zone’ in the south-east. The solutions above do not apply to these, and they require some special attention.

20.7.3 The Shadow Zone

In the fluid interior the potential vorticity of a parcel in layer 2 is determined by tracing its trajectory back to its outcrop latitude where the potential vorticity is given. That trajectory is determined by its velocity, and this in turn is determined by inverting the potential vorticity. Now, parcels subducted at y_2 sweep equatorward and westward, so that a parcel, labelled ‘ a ’ say, subducted at the eastern boundary will in general leave the eastern boundary tracing a southwestern trajectory. Consider another parcel, ‘ b ’ say, in the interior that lies eastward of the subducted position of a , in the shaded region of Fig. 20.19. It is impossible to trace b back to the outcrop line without

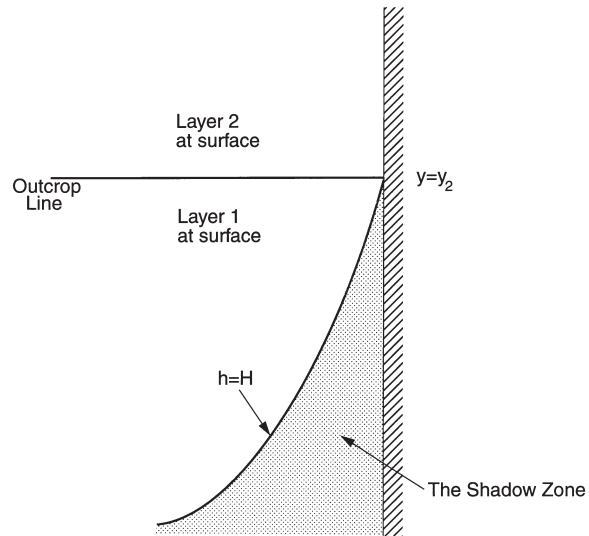


Fig. 20.19 The shadow zone in the ventilated thermocline. Layer 2 outcrops at $y = y_2$. A column moving equatorward along the eastern boundary in layer 2 is subducted at y_2 .

The column cannot remain against the eastern wall and both preserve its potential vorticity, which implies the column shrinks, at the same time that the no-normal flow condition is satisfied, as by geostrophy this implies the layer depth is constant. Thus, the column must move westward, along the boundary of a 'shadow zone' within which there is no motion. The streamline it follows is the one of constant total thickness of the two moving layers — see (20.128) or (20.130c).

trajectories crossing, and this is forbidden in steady flow. Rather, it seems as if the trajectory of \mathbf{b} would emanate from the eastern wall. What is the potential vorticity there?

At the eastern boundary the condition of no normal flow at the boundary demands that h be constant (so that $u_2 = 0$), and h_1 be constant (so that $u_1 = 0$). But if a parcel in layer 2 moves along the boundary potential vorticity conservation demands that f/h_2 is constant, and therefore h_2 must change, contradicting the no-normal flow requirement. Thus, the velocity at the boundary can have neither a normal component nor a tangential component, and so we cannot trace parcels in the shaded region back to the wall. Rather, in the absence of closed trajectories (for example, eddying motion), we may assume that the shaded region is stagnant, and h is constant. Of course, potential vorticity is everywhere given by f/h_2 , which varies spatially, but since there is no motion potential vorticity is still, rather trivially, conserved along trajectories. This region is aptly called the *shadow zone*, since the region falls under the shadow of the eastern boundary; an analogous region arose in the quasi-geostrophic discussion of Section 20.1.

To obtain an expression for the fields within the shadow zone, first note that because h is constant, its value is equal to that on the eastern wall; that is, $h = H_e$. The wind forcing must then all be taken up by the upper layer, and Sverdrup balance then implies

$$\beta v_1 h_1 = f w_E, \quad (20.106)$$

and using (20.101) we obtain an expression for h_1 , to wit

$$h_1^2 = -\frac{2f^2}{\beta g'_1} \int_x^{x_e} w_E(x', y) dx' = \frac{g'_2}{g'_1} D_0^2, \quad (20.107)$$

which is zero at the eastern wall. In the lower layer the thickness is just $h_2 = H_e - h_1$. The boundary of the shadow zone is given by the trajectory of a fluid parcel in layer 2 that emanates from the eastern boundary at the outcrop line where $h_1 = 0$ and $h = h_2 = H_e$. Since the flow is steady, the trajectory is an isoline of h . Thus, from (20.105) we have

$$h^2 = \frac{(D_0^2(x_s, y_s) + H_e^2)}{[1 + g'_1/g'_2(1 - f/f_2)^2]} = H_e^2, \quad (20.108)$$

where (x_s, y_s) denotes the boundary of the shadow zone. (Note that $x_s = x_e$ at $y = y_2$.) The above

equation yields

$$D_0^2(x_s, y_s) = H_e^2 \left[\frac{g'_1}{g'_2} \left(1 - \frac{f}{f_2} \right)^2 \right], \quad (20.109)$$

which, given the wind stress, determines the shadow zone boundary x_s as a function of y .

20.7.4† The Western Pool

Polewards of the outcrop latitude the fluid of layer 2 feels the wind directly and the layer thickness is determined by Sverdrup balance. Equatorward of the outcrop latitude the properties of this layer are determined by potential vorticity conservation, with the potential vorticity being determined by the layer thickness at the outcrop. However, just as there is a region in the east where trajectories cannot be traced back to the outcrop, there is a ‘pool’ region in the west that is bounded by the trajectory that emerges from the western boundary at the outcrop latitude. Within the pool, trajectories cannot be traced back to the outcrop (Fig. 20.18), and one might suppose that they emerge from the western boundary current. There are two plausible hypotheses for determining the layer depths within this region:

- (i) Within layer 2, potential vorticity is homogenized.
- (ii) Because there is no source for layer-2 water, layer-2 water does not exist and the pool consists solely of ventilated, layer-1 water.

Neither of the above can be derived from the governing equations of motion without making additional physical assumptions that are neither a priori true nor obvious. We discuss both hypotheses briefly below, followed by a more general discussion of how the pool region fits together with the earlier discussions about potential vorticity homogenization in the quasi-geostrophic equations.

(i) Potential vorticity homogenization

The pool region is a region of recirculation, receiving water from and depositing water into the western boundary current. Thus, following the ideas described in Chapter 13 and employed in Section 20.1, we hypothesize that the potential vorticity within this region becomes homogenized. The value of potential vorticity within the pool is just the value of potential vorticity at its boundary, and this is given by $f_2/h_2(w)$, where $h_2(w)$ is the thickness of layer 2 at the western boundary at the outcrop latitude. This is given using (20.92) with $f = f_2$ and $g' = g'_2$, and thus the potential vorticity in the pool is given by

$$q_{pool} = \frac{f_2}{D_w^2 + H_e^2}, \quad (20.110)$$

where $D_w^2 = -2(f_2^2/g'_2\beta) \int_{x_w}^{x_e} w_E(x', y_2) dx'$. The thickness of layer 2 in the pool must be consistent with this, and so is given by

$$h_2 = \frac{f}{q_{pool}}. \quad (20.111)$$

The thickness of layer 1 is determined by using Sverdrup balance, (20.100), which, given h_2 and geostrophy, reduces to an equation for h_1 , and solutions are shown in Fig. 20.20.

The extent of the pool region is dependent upon the outcrop latitude of the moving layer, since the boundary of the pool is a thickness contour. As the outcrop latitude moves poleward toward the gyre boundary then the pool region expands, as seen in Fig. 20.21. By the same token, if we have more moving layers then, since the deeper layers outcrop further poleward (Fig. 20.17) those deeper layers will have a more extensive pool region. That is, the pool expands with depth and the layer that outcrops just equatorward of the gyre boundary may have a pool region reaching across the gyre, as illustrated in Fig. 20.22, which shows the pool boundaries in a calculation (not shown here) with a three-layer model.

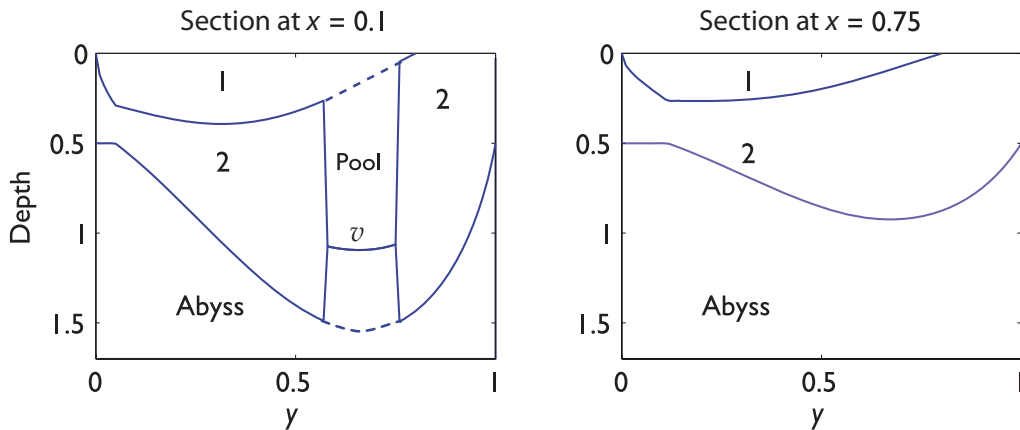


Fig. 20.20 Two north-south sections of layer thickness, at different longitudes, from the same solution as Fig. 20.18. The numbers refer to the fluid layer. The section on the left passes through the western pool region. In the homogenized PV model of the pool, the dashed lines should be solid and the line labelled v should be removed. In the ventilated pool model, the dashed lines should be removed. The region near $y = 0$ in both plots where the total depth of the thermocline is constant is the shadow zone.

(ii) The ventilated pool

'I came for the waters.' 'What waters?' 'I was misinformed.'

From Casablanca (1942).

The homogenization hypothesis, although entirely plausible, depends on the assumption of down-gradient diffusion of potential vorticity by eddies. Also, because there is no source of layer-2 water in the pool, we must suppose that it is ventilated by eddy pathways that meander down from the surface. An alternative hypothesis, and one that does not rely on the properties of mesoscale eddies, is to suppose that the western pool is filled with water that is directly ventilated from the surface. That is, if there is no surface source for a water mass, we simply suppose that that water mass does not exist. In the two-layer model, this means that the western pool is filled entirely with layer-1 fluid. If a non-ventilated (e.g., layer-2) fluid is present initially, then we hypothesize that it is slowly expunged by the continuous downwards Ekman pumping of layer-1 water into the pool.¹⁷

Because the layer-2 fluid is absent, the layer-1 fluid extends all the way down to the stagnant abyss; it takes up all the Sverdrup transport, and this determines the depth of the ventilated pool. Thus, rounding up the usual equations, we set $h = h_1$ in (20.104) to give

$$h_1^2 = D_1^2 + g'_2 H_e^2, \quad (20.112)$$

where

$$D_1^2(x, y) = -\frac{2f^2}{\beta g'_{1a}} \int_x^{x_e} w_E(x', y) dx', \quad (20.113)$$

with $g'_{1a} = g'_1 + g'_2$ being the reduced gravity between layer 1 and the abyss, and H_e , as before, being the thickness of layer 2 at the eastern boundary. Because $g'_{1a} > g'_2$ this pool will generally be shallower than the total depth of the moving fluid ($h_1 + h_2$) just outside, but the depth of layer-1 fluid alone will be much greater; that is, there will be discontinuities in layer depths at the pool boundary. A section through the pool region is shown in Fig. 20.20. The figure also shows the configuration of the pool if the homogenized potential vorticity hypothesis is used.

Although we may be shocked by the appearance of discontinuities in layer depths in a fluid model, the model does provide a simple mechanism for the appearance of *mode water*. This is a

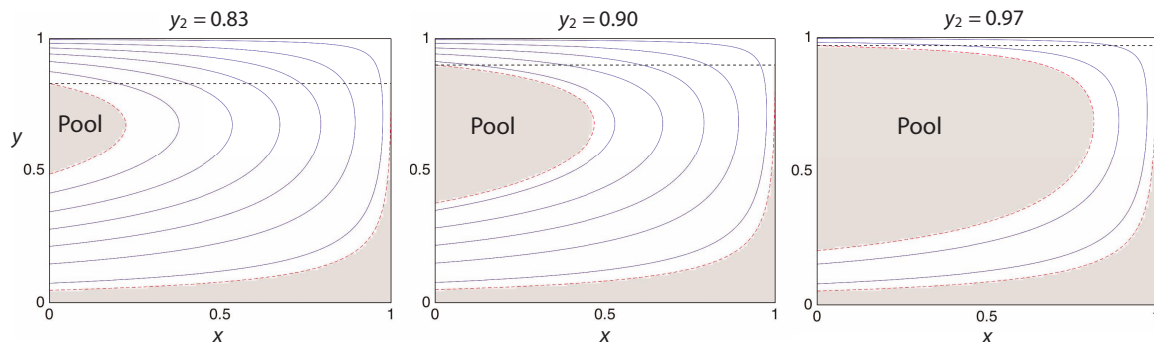


Fig. 20.21 Contour plots of total thickness in a two-layer model of the ventilated thermocline, with parameters as in Fig. 20.18, except for the outcrop latitude, y_2 , that takes values as indicated. The pool and the shadow zone are shaded and contours within are not shown. The pool expands considerably as the outcrop latitude approaches the gyre boundary at $y = 1$.

distinct mass of weakly stratified, low potential vorticity water appearing in the north-west corner of the North Atlantic subtropical gyre (where it is sometimes called ‘18 degree water’), with analogues in the other gyres of the world’s oceans; it is so-called because it appears as a distinct mode in a census of water properties. The proximate mechanism for mode water formation is convection in winter, but for such convection to occur the large-scale ocean circulation must maintain a weakly stratified region, and it is the ventilated pool that enables this, and sets the formation in the context of thermocline structure. In reality, the vertical isopycnals predicted by the simple model will be highly baroclinically unstable, and the ensuing mesoscale eddies will erode the pool interface and cause the isopycnals to slump, so that the discontinuities in layer depths will be manifest only as rapid changes or fronts.

Observations show that mode water exists only over a small region in the northeastern corner of the subtropical gyre, as the pool region in Fig. 20.18 might suggest. Regions of potential vorticity homogenization can extend much further, as in Fig. 20.4, with a similar degree of homogenization in the Atlantic. It may be that the effects of the wind are only able to homogenize the water masses in the upper regions of the pool. At greater depths the effects of baroclinic instability and the consequent mesoscale eddies may dominate the wind effects and produce regions of homogenized potential vorticity of greater horizontal extent.

20.7.5† Remarks on Thermocline Structure

In the first two sections of this chapter we discussed a quasi-geostrophic, wind-driven view of the upper thermocline and found potentially large regions in which the flow re-circulated and potential vorticity was homogenized. One might call this an *elliptic* view of the upper ocean circulation, with the value of potential vorticity being determined by a diffusion problem, with potential vorticity diffusion along isopycnals. We then discussed the thermocline in a rather different way: in the ventilated thermocline the potential vorticity is subducted in from the surface, more along the lines of a *hyperbolic* problem or a problem in characteristics. The ventilated region has an unavoidably *diffusive* internal boundary layer at its base, with diffusion across isopycnals connecting the thermocline to the abyss.

These are not necessarily competing theories; rather, the three regions (an elliptic region of potential vorticity homogenization, the hyperbolic ventilated thermocline and a diffusive internal thermocline) can co-exist in the upper ocean, as sketched in Fig. 20.15. Depending on the value of the diapycnal diffusivity, the diffusive and internal thermoclines may be almost indistinguishable, observationally if not dynamically, and, depending on the stratification and wind structure the

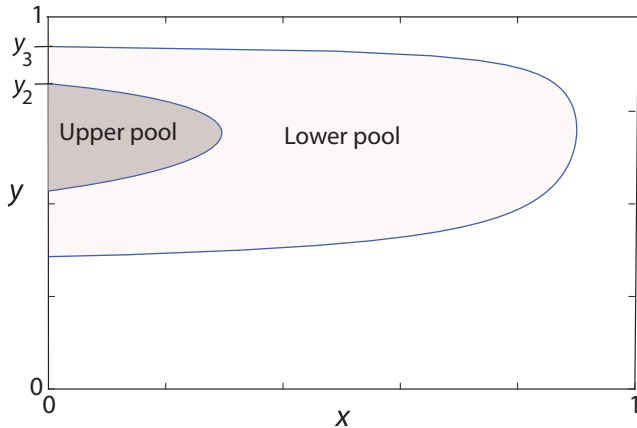


Fig. 20.22 The two pool regions in a calculation of the ventilated thermocline with three moving layers. The upper pool refers to the western pool in layer 2, which is the upper subducted layer that outcrops at y_2 , and the lower pool is that in layer 3, which outcrops at y_3 (see right-hand panel of Fig. 20.17).

regions of potential vorticity homogenization may be larger or smaller.

Finally we remark that potential vorticity is not a passive scalar, which means that the boundary of the pool region will be affected by the homogenization process. This process may entrain additional water into the pool, which then grows and may prevent subducted water from entering into it, and the edge of the homogenized region will then become a mixing barrier. However, the picture of if and how the homogenization of potential vorticity precisely affects the structure of the ventilated thermocline is a little murky, and transparency will require high resolution numerical simulations and more complete observations to guide us to the truth, or an approximation of it.

APPENDIX A: MISCELLANEOUS RELATIONSHIPS IN A LAYERED MODEL

Here we collect various expressions relating pressure, density and velocity in a geostrophic and Boussinesq layered model. The layers and the interfaces are numbered, increasing downwards, as in Fig. 20.23, and the bottom layer is stationary.

A.1 Hydrostatic Balance

Hydrostatic balance is $\partial p / \partial z = -\rho g$. We can integrate this to give, in layers n and $n-1$,

$$p_n = -\rho_n g z + p'_n(x, y), \quad p_{n-1} = -\rho_{n-1} g z + p'_{n-1}(x, y). \quad (20.114)$$

Since pressure is continuous, at $z = z_{n-1}$ these two expressions are equal so that

$$-\rho_n g z_{n-1} + p'_n = p_{n-1} = -\rho_{n-1} g z_{n-1} + p'_{n-1} \quad (20.115)$$

whence

$$g'_{n-1} z_{n-1} = \frac{1}{\rho_0} (p'_n - p'_{n-1}) \quad (20.116)$$

where $g'_n = g(\rho_{n+1} - \rho_n)/\rho_0$ is the *reduced gravity*, and ρ_0 is the constant, reference, value of the density used in the Boussinesq approximation, taken to be equal to ρ_1 .

A.2 Geostrophic and Thermal Wind Balance

In the Boussinesq approximation, geostrophic balance is:

$$\rho_0 f \mathbf{u}_n = \mathbf{k} \times \nabla p_n. \quad (20.117)$$

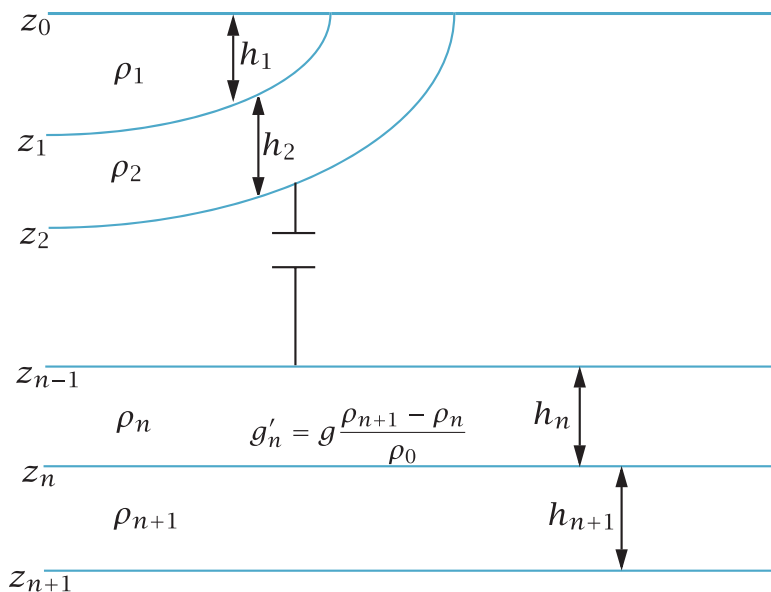


Fig. 20.23 Structure and notational conventions used for a multi-layered model.

Using (20.117) with (20.116) gives

$$\mathbf{u}_{n+1} - \mathbf{u}_n = \frac{g'_n}{f} \mathbf{k} \times \nabla z_n, \quad (20.118)$$

which is the appropriate form of thermal wind balance for this system. Let us suppose that at sufficient depth there is no motion, and in particular that layer $N + 1$ is stationary and contains no pressure gradients. That is, $p'_{N+1} = 0$ and so, from (20.115) and (20.117)

$$p'_N = -(\rho_{N+1} - \rho_N)gz_N = -g'_N \rho_0 z_N. \quad (20.119)$$

Integrating upwards we obtain the pressure in each layer,

$$p'_n = -\rho_0 \sum_{i=n}^{i=N} g'_i z_i \quad (20.120)$$

where $n \leq N$. Thus, the geostrophic velocities in each layer are given by

$$f\mathbf{u}_n = -\mathbf{k} \times \nabla \left(\sum_{i=n}^{i=N} g'_i z_i \right). \quad (20.121)$$

The quantity in brackets on the right-hand side is not a velocity streamfunction because it is $f\mathbf{u}_n$, and not \mathbf{u}_n that is given by its curl. Nevertheless, the velocity is normal to its gradient, and therefore its isolines define streamlines.

The upper surface of the ocean is assumed to be fixed; this is the ‘rigid-lid’ approximation. Thus, $z_0 = 0$ and $h_1 = -z_1$. More generally, the layer thicknesses and the interfaces between the layers are related by

$$z_n = - \sum_{i=M}^{i=n} h_i \quad (20.122)$$

where M is the index of the uppermost layer, and $n \geq M$. If there is no outcropping, then $M = 1$.

The geostrophic velocity in the lowest moving layer is given by

$$f\mathbf{u}_N = -g'_N \mathbf{k} \times \nabla z_N = g'_N \mathbf{k} \times \nabla h. \quad (20.123)$$

This means that lines of constant depth of the lowest layer are also streamlines; the velocity moves parallel to the depth contours. The vertical velocity at the base of the lowest layer is given by, for steady flow,

$$w(z = -h) = \mathbf{u}_N \cdot \nabla h = \frac{1}{f} g'_N (\mathbf{k} \times \nabla h) \cdot \nabla h = 0. \quad (20.124)$$

That is, there is no vertical motion at the base of the moving layers.

A.3 Explicit Cases

A one-layer reduced-gravity model

The perturbation pressure in the moving layer (layer 1) is

$$p'_1 = -\rho_0 g'_1 z_1 = \rho_0 g'_1 h_1. \quad (20.125)$$

The geostrophic velocity is given by

$$f\mathbf{u}_1 = \frac{1}{\rho_0} \mathbf{k} \times \nabla p'_1 = g'_1 \mathbf{k} \times \nabla h_1. \quad (20.126)$$

(In a single-layer model, the subscripts are often omitted.)

A two-layer model

The perturbation pressures in the upper and lower moving layers are given by

$$p'_1 = -\rho_0 (g'_2 z_2 + g'_1 z_1) = \rho_0 (g'_2 h + g'_1 h_1), \quad (20.127a)$$

$$p'_2 = -\rho_0 g'_2 z_2 = \rho_0 g'_2 (h_1 + h_2) = \rho_0 g'_2 h, \quad (20.127b)$$

where $h = h_1 + h_2 = -z_2$.

The corresponding geostrophic velocities are

$$f\mathbf{u}_1 = \mathbf{k} \times \nabla (g'_2 h + g'_1 h_1), \quad (20.128a)$$

$$f\mathbf{u}_2 = \mathbf{k} \times \nabla (g'_2 h). \quad (20.128b)$$

A three-layer model

The perturbation pressures in the three moving layers are

$$p_1 = -\rho_0 [g'_3 z_3 + g'_2 z_2 + g'_1 z_1] = \rho_0 [g'_3 h + g'_2 (h_1 + h_2) + g'_1 h_1], \quad (20.129a)$$

$$p_2 = -\rho_0 [g'_2 z_2 + g'_3 z_3] = \rho_0 [g'_2 (h_1 + h_2) + g'_3 h], \quad (20.129b)$$

$$p_3 = -\rho_0 g'_3 z_3 = \rho_0 g'_3 h, \quad (20.129c)$$

where $h = h_1 + h_2 + h_3 = -z_3$. The corresponding geostrophic velocities are:

$$f\mathbf{u}_1 = \mathbf{k} \times \nabla [g'_3 h + g'_2 (h_1 + h_2) + g'_1 h_1] \quad (20.130a)$$

$$f\mathbf{u}_2 = \mathbf{k} \times \nabla [g'_2 (h_1 + h_2) + g'_3 h] \quad (20.130b)$$

$$f\mathbf{u}_3 = \mathbf{k} \times \nabla [g'_3 h]. \quad (20.130c)$$

Notes

- 1 Drawing from Rhines & Young (1982b). Young & Rhines (1982) also considered the problem of a western boundary layer.
- 2 Indian Ocean results are from McCarthy & Talley (1999), and I am very grateful to Lynne Talley for the Pacific plots. The data is mainly from CTD profiles and bottle casts. The potential density is σ_0 in the upper ocean plots, and σ_2 for the deep ocean.
- 3 See Rhines & Young (1982a) and Holland *et al.* (1984) for numerical examples of PV homogenization and Xu *et al.* (2015) for some related high-resolution simulations of the Atlantic.
- 4 I am very grateful to Peter Rhines for constructing Figs. 20.5, 20.6 and 20.7 from MIMOC data, and for his insightful interpretations. The MIMOC climatology is described at <http://www.pmel.noaa.gov/mimoc/> and by Schmidtko *et al.* (2013). The date comes mainly from Argo CTDs, supplemented by shipboard and ice-tethered profiler CTDs, and is put onto a 0.5° grid.
- 5 See Keffer (1985), Talley (1988), Lozier *et al.* (1996) and McCarthy & Talley (1999) for some earlier observations of potential vorticity.
- 6 Sections courtesy of L. Talley and the WOCE hydrographic atlas. Globally continuous, unique, neutral-density surfaces cannot be constructed exactly because of the presence of salinity and the thermobaric term in the equation of state for seawater, and a parcel will not necessarily return to its level of departure when displaced to the same (x, y) position. Neutral density is nonetheless useful, and for the purposes of this figure it is the same as potential density.
- 7 See, among others, Toole *et al.* (1994), Polzin *et al.* (1997), Gregg (1998) and Ledwell *et al.* (1998).
- 8 For estimates of the strength of the overturning circulation in the ocean, and its relation to diapycnal diffusivity and the observed stratification, see Munk (1966), revisited by Munk & Wunsch (1998) and Wunsch & Ferrari (2004). If the abyssal flow is along rather than across isopycnals, smaller values of diffusivity suffice to maintain deep stratification — see Section 21.6.
- 9 Vallis (2000).
- 10 The modern development of the theory of the main thermocline began with two back-to-back papers in 1959 in the journal *Tellus*. Welander (1959) suggested an adiabatic model, based on the ideal-fluid thermocline equations (i.e., the planetary-geostrophic equations, with no diffusion terms in the buoyancy equation), whereas Robinson & Stommel (1959) proposed a model that is intrinsically diffusive. In this model (developed further by Stommel & Webster (1963), Salmon (1990), and others) the thermocline is an internal boundary layer or front that forms at the convergence of two different homogeneous water types, warm surface fluid above and cold abyssal fluid below. Meanwhile, the adiabatic model continued its own development (see Veronis 1969), culminating in the ventilated thermocline model of Luyten *et al.* (1983) and its continuous extensions (e.g., Killworth 1987). Signs that the two classes of theory might not be wholly incompatible came from Welander (1971b) and Colin de Verdier (1989) who noted that the diffusion might become important below an adiabatic near-surface flow, and Samelson & Vallis (1997) eventually suggested a model in which the upper thermocline is adiabatic, as in the ventilated thermocline model, but has a diffusive base, constituting an internal boundary layer. Mesoscale eddies play a role in homogenizing potential vorticity in the pool regions (e.g. Henning & Vallis 2004, Cessi & Fantini 2004, Maze & Marshall 2011). Extensions of the ventilated-style of model to the subpolar gyre are provided by Bell (2015b,a).
- 11 Welander (1971a).
- 12 Drawing from Salmon (1990).
- 13 Newton's method is an iterative way to numerically solve certain types of differential equations. The solutions here are obtained using about 1000 uniformly spaced grid points to span the domain, taking just a few seconds of computer time. Because of the boundary layer structure of the solutions employing a non-uniform grid would be even more efficient for this problem, but there is little point in designing a streamlined hat to reduce the effort of walking.
- 14 Following Samelson (1999b).

- 15 Following Luyten *et al.* (1983).
- 16 It may be that the eastern boundary depth is determined by global thermodynamic and/or mass constraints; see, for example, Boccaletti *et al.* (2004). There must also be a poleward transport across the boundary of the subtropical–subpolar gyre to balance the equatorward transport in the Ekman layer and that of the meridional overturning circulation, and this balance requirement may influence the boundary depth.
- 17 Dewar *et al.* (2005). This paper also discusses the nature of discontinuities at the pool boundaries, and their treatment via shock conditions.

In the shadow zone, layer-2 fluid also has no direct surface source, so one may wonder why this is also not expunged. However, the shadow zone is not a recirculating regime and the Ekman induced displacement will be much less efficient. More directly, the eastern boundary condition $h_1(x = x_e) = 0$ precludes the vanishing of layer-2 water there, and this boundary condition is propagated westwards into the interior.